TÉCNICO LISBOA

Development of a Regenerative CO_2 Air Capture Process for Sustainable Greenhouses

Simone Morgana Gorny

Thesis to obtain the Master of Science Degree in

Biological Engineering

Supervisors: Dr.ir. Derk Willem Frederik Brilman
Prof. Dr. Helena Maria Rodrigues Vasconcelos Pinheiro

Examination Committee

Chairperson: Prof. Dr. Marília Clemente Velez Mateus
Supervisor: Prof. Dr. Helena Maria Rodrigues Vasconcelos Pinheiro
Members of the Committee: Prof. Dr. Sebastião Manuel Tavares da Silva Alves

October 2019

Preface

The work presented in this thesis was performed at the Sustainable Process Technology (SPT) Group of the University of Twente (Enschede, The Netherlands), during the period February-August 2019, under the supervision of Michel Schellevis (MSc, PhD Candidate) and Dr.ir. Wim Brilman (Associate Professor), and within the frame of the Erasmus programme. The thesis was co-supervised at Instituto Superior Técnico by Prof. Helena Pinheiro.

I declare that this document is an original work of my own authorship and that it fulfils all the requirements of the Code of Conduct and Good Practices of the Universidade de Lisboa

Abstract

Climate change due to global warming is a major issue in the present day and age, and one of the biggest challenges to be overcome as a society. Within the scientific community, it is accepted (and mostly a given fact) that anthropogenic CO_2 emissions are a main contributor. Atmospheric levels of CO_2 have risen since the Industrial Revolution and will keep on rising if the current emissions are maintained. So, it is vastly important to reduce emissions, in order to stabilize the level of CO_2 in the atmosphere. CO_2 capturing technologies have the advantage of not only allowing the reduction of emissions, but also of removing CO_2 from ambient air, a technology called Direct Air Capture. Adsorption of CO_2 on solid amine sorbents is one of the leading methods of capturing CO_2.

This work takes the first steps towards designing an installation that captures CO_2 from ambient air using Lewatit® VP OC 1065 (a solid amine sorbent) to produce a continuous stream of CO_2 enriched air at a flow rate of 1 kg_{CO_2}/h, to be installed in a greenhouse, where the product stream is used to enrich the air under the leaves of the crops, to promote their growth.

Three types of contactor reactors where considered: axial flow fixed bed, radial flow fixed bed, and fluidized bed. Preliminary cost calculations showed that a fluidized bed is the most economic choice for an installation of this scale.

In order to determine the most favourable operation parameters in a fluidized bed, the uptake rate of CO_2 and the contact efficiency between the solid phase and the gas phase were analysed and compared from breakthrough curves of CO_2 adsorption obtained in a single stage fluidized bed, for different superficial velocities, bed heights and concentrations of CO_2. Based on these results, a design of a setup was developed.

In the final design, 1×10^3 m^3/h (20°C,1 atm) of ambient air are divided between 10 fluidized beds stacked on top of each other, at room temperature, while the sorbent circulates from the top stage to the bottom one, through pipes that connect the stages. Each stage has a 40 cm diameter and 10 cm height. The sorbent, loaded with CO_2, leaves the bottom stage and flows into the desorber, a multistage fluidized bed with only one air stream as purge. The desorber is at a constant temperature of 70°C, temperature at which the CO_2 is released from the sorbent and subsequently transported by the purge stream. This results in a product stream of CO_2 enriched air, with a concentration between 0.5 and 1% (v/v). The lean sorbent is recycled back into the top stage of the adsorber.

For the final design, operational costs where determined, reaching an estimate of 240 €/ton_{CO_2}. This is higher than the cost of industrial CO_2, which varies between 80 and 180 €/ton_{CO_2}. However, the calculations where done under a pessimistic scenario, and therefore the operation cost of the designed installation is likely to be lower. Besides this point, the design is a first draft, that would require further studies and modeling before reaching a final, more cost effective, plan.

Keywords: CO_2, direct air capture, adsorption, amine sorbent, sustainable greenhouses

Resumo

As alterações climáticas devido ao aquecimento global são um grande problema hoje em dia, e um dos maiores desafios a superar como sociedade. Dentro da comunidade científica, é geralmente aceite que as emissões antropogénicas de CO_2 são uma das principais contribuições. Os níveis atmosféricos de CO_2 têm subido desde a Revolução Industrial, e continuarão a subir se as emissões atuais se mantiverem. Por isso, é muito importante reduzir as emissões de forma a estabilizar o nível de CO_2 na atmosfera. As tecnologias de captura de CO_2 têm a vantagem de não só permitir a redução de emissões, mas também de remover CO_2 de ar ambiente, uma tecnologia denominada *Direct Air Capture*. A adsorção de CO_2 em adsorventes sólidos com grupos amina é um dos métodos de captura de CO_2 mais promissores.

Esta tese dá os primeiros passos no sentido de dimensionar uma instalação que captura CO_2 do ar ambiente usando Lewatit® VP OC 1065 (um adsorvente sólido com grupos amina) para produzir uma corrente contínua de ar rico em CO_2 com um caudal de 1 kg_{CO_2}/h, para ser instalado numa estufa, onde a corrente resultante é usada para enriquecer o ar da parte de baixo das folhas da plantação, para promover o seu crescimento.

Três tipos de reator foram considerados: leito fixo de fluxo axial, leito fixo de fluxo radial, e leito fluidizado. Cálculos preliminares de custos revelaram que o reator de leito fluidizado é a escolha mais económica para uma instalação a esta escala.

De forma a determinar os parâmetros de operação mais favoráveis num reator de leito fluidizado, a taxa de adsorção de CO_2 e a eficiência do contacto entre a fase sólida e a fasa gasosa foram analisados e comparados a partir das curvas de saturação do processo de adsorção de CO_2 num único leito fixo, para diferentes velocidades superficiais, alturas do leito e concentrações de CO_2. Com base nestes resultados, foi desenvolvido um desenho de uma instalação.

No desenho final, 1×10^3 m^3/h (20°C,1 atm) de ar ambiente são divididos por 10 andares de leito fixo empilhados, à temperatura ambiente, enquanto que o adsorvente circula de andar superior ao andar inferior através de tubos que ligam andares consecutivos. Cada andar tem 40 cm de diâmetro e 10 cm de altura. O adsorvente, carregado de CO_2, sai do andar inferior para a coluna de desadsorção, um leito fluidizado de andares múltiplos com uma única corrente de ar de purga. A coluna de desadsorção tem uma temperatura constante de 70°C, temperatura à qual o CO_2 é libertado do adsorvente e consequentemente transportado pelo ar de purga. Este processo resulta numa corrente produto de ar rico em CO_2, com concentrações entre 0.5 e 1% (v/v). O adsorvente, pós desadsorção, é recirculado para o andar superior da coluna de adsorção.

Para o desenho final, foram determinados os custos de operação, resultando num custo estimado de 240 €/ton_{CO_2}. Este custo é superior ao custo de CO_2 industrial, que varia entre 80 e 180 €/ton_{CO_2}. Porém, estes cálculos foram feitos num cenário pessimista, pelo que os custos de operação desta instalação poderão ser mais baixos. Para além disto, o desenho descrito é um desenho inicial, que requer estudos posteriores e modelação antes de se atingir um desenho final, mais economicamente viável.

Keywords: CO_2, captura direta do ar, adsorção, adsorventes com grupos amina, estufas sustentáveis

Contents

List of Tables

List of Figures

1 Introduction

CO_2 emissions

Large carbon dioxide (CO_2) emissions due to human activities are known to cause the climate changes that are already apparent this day and age, and are only prone to become worse. It is crucial to stabilize the levels of CO_2 in the atmosphere, as the average concentration of CO_2 has already increased from 280 ppm during the pre-industrial time to over 400 ppm presently [4], and half of the already emitted CO_2 will remain there for centuries [5]. The alarming rate the CO_2 concentration increased over the last two and a half centuries can be seen in Figure 1.1. If the carbon in all of the estimated fossil fuel reserves was emitted to the atmosphere, the carbon concentration would rise to more than 5 times the pre-industrial levels. Based on the prediction of the Intergovenmental Panel on Climate Chage (IPCC), by the year 2100, the atmosphere may contain up to 570 ppm of CO_2, causing a rise of mean global temperature of around 1.9°C and an increase in average sea level of 3.8 m. The IPCC special report on CO_2 capture and storage attributes 60% of global CO_2 emission in 2000 to a majority of electrical power stations. The remaining 40% emissions were mainly from transportation systems. [6]

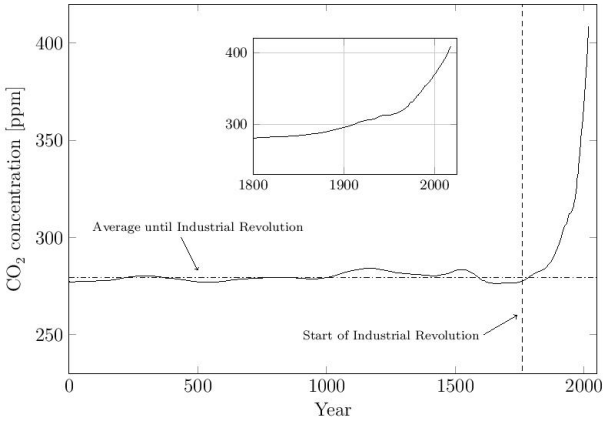

Figure 1.1: Evolution of the average CO_2 concentration in the atmosphere over the last 2000 years.

Due to these dire prospects, strategies to reduce the amount of CO_2 released into the atmosphere are essential, in order to stabilize its level. By 2050, CO_2 emissions need to be reduced by 30-85% to be on track to stabilize atmospheric CO_2 between 350 and 440 ppm [5]. These strategies begin with reducing the use of fossil fuels, mainly eliminating the emissions from coal, and decreasing amounts produced by other fuels which have high carbon footprints. It is fundamental that this happens in the next few decades. Beyond 2050, CO_2 emissions must continue to decrease to levels approaching zero, towards a full stabilization of atmospheric CO_2. Even then, it may be necessary to reduce the amount of CO_2 in the atmosphere below the current level, or future stabilization level [5]. However, the switch to carbon free and renewable energy sources poses many socio-economic and political obstacles, due to costs and low environmental mindset of the general population and many political leaders. Even though it is theoretically possible to supply the energy necessary for human activities through them [5], at the current state of development of the renewable energy technologies it is not possible to meet the energy demands of the population with renewable or clean energy sources [6]. Besides this, the disruption of the existing infrastructure and supply network is not possible in a short time without harsh consequences to the global economy [6]. Therefore, to "buy time" and allow the switch to clean energy

sources to be done at a pace that will not tarnish the economy and does not render the current infrastructure useless, there are several ways of reducing the carbon emissions of the current and existing power plants.

The Carbon Capture and Storage (CCS) technology was developed for this purpose. This technology, in one of its most developed methods, uses the reversible reaction of CO_2 with amines to remove the CO_2 from a gas stream, and compress it into empty natural gas reservoirs. This will be further explained in chapter 2 (Scientific Background). The advantage of CO_2 capture is that it can be retrofitted to existing facilities, without significant changes to the infrastructure of the energy plant [7] or to the current process, or to the consumers, which is beneficial considering the societal inertia in dealing with climate change [5].

Even though carbon capture and storage prevents CO_2 release into the atmosphere and is a good option for mitigation of global warming, its storage can present a further issue. The main storage place is former underground natural gas reservoirs, meaning, the geological formations where natural gas was trapped in for millions of years. It can be argued that natural gas was kept there without leaks for a long time, and that a leak in these storage places is equivalent to a leak in a pipeline. However, storage space, even though abundant, is limited and has associated costs of compression, transportation to the storage sites and pumping. Besides, there are not enough storage sites to store all the CO_2 captured from all the fossil fuels still to be used [8]. Therefore, this technology, when used in power plants, cannot be used as a solution to global warming, but rather as a mitigation strategy to support the transition to clean renewable energy.

CO_2 capture is not limited to flue gases, as it can also be applied to direct air capture (DAC). CO_2 capture from ambient air is one of the few options to mitigate emissions from distributed sources, which account for one-third to half of the total anthropogenic CO_2 emissions. Air capture could deal with automobile and airplane emissions, which cannot be obtained from regular CCS and also mitigate residual emissions from CCS, dealing with fugitive emissions during transport and storage and manage leakages at the storage sites. [5]

As there is a market for CO_2, the carbon capture technology can be joined to the CO_2 needs in several industries that have use for it. For instance, if it is possible to produce food-grade CO_2 using this technology, the captured CO_2 can be used in the carbonated beverages industry. If CO_2 becomes the carbon source for the industry, as some believe, this technology will be its basis. Another use for it, and which is already done in some specific cases in the Netherlands, is in industrial greenhouses, where CO_2 is supplied to achieve a higher concentration in the air, which increases the productivity of the cultures, all year round. Other uses for CO_2 include urea production, fertilizer production, foam blowing and dry ice production [6].

Greenhouse sustainability

A lot of the food supply nowadays is cultivated in greenhouses, seeing as there are many advantages in growing crops and other plants in closed controlled setups as opposed to directly exposed to the atmosphere. Besides the obvious protection from atmospheric conditions like rain, wind, snow, intense sunlight, etc., the greenhouse allows a control over the temperature, air humidity, intensity and hours of light exposure, air compositions, and avoiding plagues and cross pollination.

However, as any closed space, climate control is important. Lack of it in many greenhouses results in an inadequate micro-climate that impacts yields and input-use efficiency of the crops. A good control of the climate of the greenhouse can lead to higher yields and better quality of the crops, and even extend the growing season to all year round. As plants assimilate CO_2, its concentration in the greenhouse environment is a relevant parameter to control. The atmospheric concentration of CO_2 is limiting to the potential productivity of most plant species, and, in a closed space like a greenhouse, the CO_2 consumption rate can be higher than the supply rate through the ventilation system and therefore the CO_2 concentration drops below atmospheric levels. A low efficiency of ventilation combined with the use of insect-proof nets in many greenhouses leads to a reduction of up to 20% or more of the atmospheric levels of CO_2, which severely affects the productivity.

Solutions to this are an improved the design of the ventilation system, to use forced air ventilation, or to provide CO_2 enriched air. In Northern Europe, CO_2 enrichment is a common practice to enhance crop productivity during low radiation conditions. Crop yield and quality increases under enrichments of CO_2 to ambient air concentrations of 700-900 ppm. This is possible in the Northern countries of Europe, which do not require that much ventilation with the purpose of lowering the temperature. In Southern European countries, on the other hand, greenhouses require more ventilation due to the overall higher temperatures. Because of this, more CO_2 is lost and it is uneconomical to maintain these levels of CO_2. Under these conditions, some authors recommend supplying CO_2 to the greenhouse to maintain atmospheric levels during the time that ventilation is operating, and increasing the levels to 700-800 ppm when the greenhouse is closed, which is usually during the early morning and late afternoon. [9]

The CO_2 can be supplied through various ways but, in Northern Europe, it is common to supply industrial CO_2 that comes in liquid form. It is heated and provided in gas form through a pipe along the roots or stems of the plants. The CCS technology can be applied here, where the CO_2 from energy plants or factories is captured and, instead of being pumped into the underground reservoirs, is transported to these greenhouses. Even though in theory this seems like a sustainable utilization of CO_2, it was revealed by a study done by Royal Roses, a rose culture greenhouse in Leidschendam, the Netherlands, that the plants use only 10% of the supplied CO_2, leaving 90% to be released into the atmosphere through ventilation. Seeing this, there is no relevant reduction in CO_2 released to the atmosphere. In greenhouses that supply CO_2 by the traditional methods, not only is there no reduction of emissions, but altogether an increase, leaving greenhouse production as an operation with a high carbon footprint. To tackle this issue, carbon capture methods and DAC can be a possible solution.

Scope of the Project

The suggested solution, and purpose of this work, is designing an air capture unit that allows the recovery and reuse of the wasted CO_2 that is still in the greenhouse ambient air, in order to supply it again to the crops. This way, the amount of CO_2 which is supplied industrially is reduced, and the carbon footprint of the culture is reduced. The goal is to reduce the supplied CO_2 by 50%.

The installation to be designed would have the air inside the greenhouse circulate through a carbon capture column before being released either into the atmosphere or back into the greenhouse. The CO_2 that is adsorbed in the column onto the sorbent is then desorbed by increase of temperature and can be recirculated into the greenhouse in either pure form or, if atmospheric air is used for purging, as CO_2-enriched air. This process is represented in Figure 1.2. This way, a lot more of the supplied CO_2 will be used by the crops, reducing the amount of industrial CO_2 needed and the amount of CO_2 released into the atmosphere. The overall objective of this thesis is to come to a design of a scalable CO_2 capture installation and process layout that can be implemented in existing greenhouses to minimize their carbon footprint.

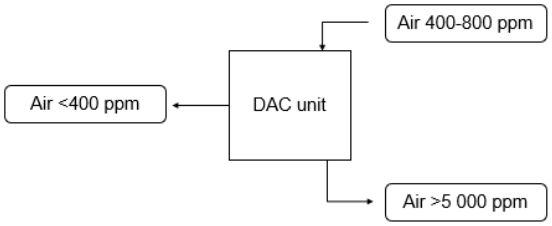

Figure 1.2: Representation of the suggested DAC unit to be designed in this work.

2 Scientific Background

2.1 Carbon Capture and Storage

To reduce the CO_2 emissions in fossil fuel combustion facilities, there are three different strategy categories, namely, pre-combustion CO_2 capture, post-combustion CO_2 capture and oxy-fuel combustion. In the pre-combustion technologies, the fuel is gasified before combustion and reacted in a water gas shift reactor to produce H_2 and CO_2 [7], generally in higher concentrations so there is a bigger driving force to separate the CO_2 subsequently. The gasification cycle can be combined with ammonia production, and this process is well established [6]. The oxy-fuel combustion technology uses nearly pure oxygen in the combustion, so mostly CO_2 and H_2O are released in the process [7], but the costs of producing pure oxygen are high [6]. In this process, CO_2 is recycled and used to expand the medium, instead of air, and to avoid excessively high combustion temperatures [6]. These two strategies have the disadvantage of requiring changes to the energy generation process and to the infrastructure of existing facilities. [7]

To achieve some reduction in the amount of CO_2 released, without significant changes to the process of combustion or infrastructure, several post-combustion CO_2 capture and storage methods have been developed. These consisted, originally, of capturing the CO_2 at the source of the pollution, like at an energy power plant, transporting it to a geological site and storing it there [10]. Before transportation, CO_2 is compressed to about 70 bar to be transported and stored in liquid form [8]. This method requires the separation of CO_2 from the flue gases because the compression and storage of the full volume of combustion gases is too costly [6]. Therefore, the switch to clean energy sources is supported in a way that decreases the impact of the current energy sources, by remedying the releases of CO_2 in existing energy plants based of fossil fuels, so the stabilization of the level of CO_2 in the atmosphere is less distant in time [7]. One of the disadvantages of the post-combustion capture is that flue gas has relatively low concentrations of CO_2, typically 4-14% by volume, thus large volumes need to be treated to obtain a significant amount of CO_2 for storage, meaning large equipment sizes and high investment costs. The design is also a challenge due to the high temperature of the flue gases. [6]

Most of the CO_2 capture methods being developed are based on either gas-liquid absorption, gas-solid adsorption or separation by a membrane [11]. The studies into these methods are very diverse, including methods based on chemisorbents, physisorbents and cryogenic techniques. Technologies using chemical sorption are being widely studied as they are highly effective and selective [10]. Processes with specialized solvents were developed over 60 years ago for CO_2 removal from impure natural gas [6] and to remove CO_2 from the air in submarines, and are still used today. The use of each of these techniques depends on several factors, namely the source and composition of the gas stream and if it is pre- or post-combustion [11], partial pressure of CO_2, extent of recovery required, regeneration of the solvent, purity desired and sensitivity to impurities, costs of the process, environmental impact, to name a few [6].

The most developed capture process is CO_2 absorption by aqueous alkanolamine solutions, where CO_2 is selectively absorbed by the reactive solvent in a scrubber. The CO_2-rich amine solvent is then sent to a stripper, where it is heated, and the CO_2 is released from the solution and compressed for transport and sequestration [7]. The most studied amine is monoethanolamine (MEA), but many others can be used, such as piperazine (PZ). The process captures CO_2 primarily via carbamate formation (equation 2.1) and bicarbonate

formation (equation 2.2).

$$2R_1R_2NH + CO_2 \leftrightarrows (R_1R_2NH_2^+)(R_1R_2NCOO^-) \tag{2.1}$$

$$R_1R_2NH + CO_2 + H_2O \leftrightarrows (R_1R_2NH_2^+)(HCO_3^-) \tag{2.2}$$

In primary amines, R_2 is a hydrogen. In the case of a terciary amine, as these have no hydrogen atoms, only reaction 2.2 can proceed (where H is substituted by R_3). During the stripping, the temperature increase drives the reaction equilibrium towards the reactants. [7]

However, this process is energy intensive due to high reboiler duty requirement of solvents used currently and the widespread application of this technology is still limited since it increases the overall cost of the energy production process [11].The operational costs associated with the thermal energy input of the amine scrubbing process make up around 44% of the total CO_2 capture costs and the total costs of the carbon capture and storage can double the cost of electricity [12]. Other disadvantages of this process include corrosion, solvent evaporation and solvent degradation [11]. Despite this, amine-based solvents are already used for CO_2 removal from natural gas and industrial exhaust gas [10].

2.2 Carbon Capture with solid sorbents

As a viable alternative to gas-liquid absorption, processes based on either physical or chemical adsorption of CO_2 by solid sorbents are currently being developed. Here, regeneration of solid sorbents requires much less energy than the solvent systems [11]. This is due to the lower heat capacity of the solid support compared to the aqueous support in an absorption process. Also, water evaporation is prevented. [12]

Solid supports for amine sorbents are highly porous materials, with a high internal surface area and functionalized amine groups either immobilized on or grafted into the surface. The aspects of these sorbents that are looked at when choosing an appropriate one are CO_2 capacities, CO_2 uptake rates, involved heats of adsorption and regeneration conditions.

In a typical adsorption separation process for CO_2 capture from a fossil-fired power plant, with solid sorbents, the CO_2 rich flue gas is contacted with a lean adsorbent at low temperature and CO_2 is preferentially adsorbed onto the material. Once the sorbent is saturated, it is then regenerated by heating the sorbent (temperature swing adsorption; TSA) or lowering the partial pressure of CO_2 (pressure swing adsorption; PSA), or some combination of the two, which causes CO_2 to desorb from the material at high purity. [13]

The material properties of the sorbent, including the adsorption isotherms and amine densities, will determine its working capacity and how much pure CO_2 can be produced for any given regeneration conditions. The quality and quantity of separation achieved is dependent on the material properties and the driving force of the regeneration, provided by the change in temperature or pressure, both of which have an associated energy cost or energy penalty on the power plant, or wherever it is being applied to. When using temperature swing, the energy penalty is associated to the heating of the sorbent for desorption. In a power plant, this can be done with steam extracted from the low pressure turbine of the main steam cycle. As the temperatures required for the regeneration are not so high (60-200°C), the loss of electrical output in the power plant as consequence of the extraction of steam is not significant. On the pressure swing, on the other hand, the energy penalty is the extra energy requirement for compressing the product CO_2 from the regeneration pressure, and this compressor work cannot be discounted in the same way as the heating requirements because compressor work imposes an electrical load on the power plant. [13]

However, in real systems, both heating requirements and compression work will be necessary in both pressure swing as in temperature swing. Thermal energy will be required in PSA processes to overcome the

endothermic regeneration of the sorbent and compression will be required in a TSA process to efficiently pressurize CO_2 to pipeline pressures of 150 bar. Therefore, the energy penalty of capturing CO_2 with solid sorbents is dependent both on the material properties of the sorbent used and on the regeneration conditions. The optimal regeneration conditions need to be determined for each material. [13]

2.3 Sorbent screening and process development

In an effort to develop a process using supported amine sorbents (SAS) with a lower energy demand than the conventional aqueous amine solvent method, Veneman [14] tested the CO_2 capacity and thermal stability of several sorbent materials, both impregnated with amines and grafted with amines. In grafted sorbents, the amines are covalently bound to the polymeric structure, while in impregnated sorbents these are bound to the sorbent by weak interactions. Impregnated amine sorbents revealed to have a higher initial capacity to adsorb CO_2, because the impregnation allows a higher density of amines than the grafting. On the other hand, grafted amine sorbents were shown to have a much higher stability, even though they have a lower capacity. Due to the degradation the impregnated amines suffer, the capacity of the impregnated sorbents decreases significantly after a relatively short use of the material, lowering below the capacity of grafted amine sorbents. One of the grafted amine sorbents tested by Veneman [14], the Lewatit® VP OC 1065 sorbent, a polystyrene based ion exchange resin (IER) containing primary benzyl amine units covalently bound to the structure, was found to be very stable and resistant to degradation and with a good capacity to adsorb CO_2 and therefore was used in further studies in the Sustainable Process Technology research group (SPT).

When designing a reactor for this process, several factors need to be taken into account. The adsorption rate of CO_2 by the amine sorbent is influenced by a combination of factors, namely external mass transfer, internal diffusion and reaction kinetics. The particle effectiveness was found to be between 60 and 70%. Heat transfer, internal or external, will not have a significant effect on the performance of the sorbent. Under flue gas conditions (T=328 K, P_{CO_2}=0.137 bar), it can take 80 seconds for the Lewatit® VP OC 1065 sorbent to be saturated. It was found that the rate of the adsorption depends highly on the concentration of CO_2 in the gas stream. [14]

Adsorption reactors can be better than the conventional solvent processes in productivity, as well as in design and energy demand. The size of the columns can be significantly reduced and energy demand is lower. These factors reduce the capital investment and operation cost of the CO_2 capture process, compared to the solvent based method. Compared to a scrubber, an adsorption column is less expensive, and, even though desorption requires heating both the sorbent and the solvent, the heat capacity of the sorbent is lower and its capacity is higher, therefore the sensible heat demand of the process is lower. [14]

2.4 Direct Air Capture

The notion of applying the carbon capture technology to ambient air, referred to as direct air capture (DAC), has been around since the early 1990s and has been subjected to research in the decades since. It is not a competitive technology to the traditional carbon capture on point source emissions, but an additional technology that provides flexibility in the mitigation of CO_2 emissions. [15]

The advantages of DAC are widespread: it can address emissions from distributed sources, which traditional CCS cannot; air contains very low to nil concentrations of contaminants present in flue gases, such as NO_x and SO_x, which prove to be a disadvantage; it can be implemented anywhere; and it can be applied to Carbon Capture and Utilization (CCU), providing CO_2 to the various industrial uses mentioned in chapter 1. [15]

However, from a thermodynamics point of view, DAC is less favourable than CO_2 capture from flue gases due to the much lower CO_2 concentration in ambient air. Nonetheless, this aspect does not present a limitation

on the economics of the DAC process [16]. As a point of reference, the determined free energy required to separate one mole of CO_2 from a gas mixture in ambient air conditions (40 Pa, 303 K, 1 atm) is 20 kJ/mol, while from power-plant derived flue gas (12 kPa, 335 K, 1 atm) is 6 kJ/mol [17]. Considering the concentration ratio is about 300, the difference in thermodynamic energy requirement between these two cases is small. [15]

Thermodynamics not being the main limitation of DAC, the massive amount of air to be treated per mass of CO_2 captured is the main challenge [15]. As large volumes of air need to be treated to obtain a meaningful amount of CO_2, air capture methods cannot be energy intensive. Therefore, the only feasible techniques are absorption or adsorption on a solvent or sorbent, respectively [5]. Several companies and research groups have developed DAC technologies, most resorting to some form of carbonate formation or carbonation-calcination cycles. One of the most promising remains the solid amine sorbents because they display relatively high CO_2 capacities and tolerance of water, moderate regeneration energy and stability under air capture conditions. [15] From these, the Lewatit® VP OC 1065 sorbent remains an appropriate sorbent for carbon capture, even to be used in processes which use ambient air.

2.5 DAC for sustainable greenhouses

There are many ways of providing CO_2 to greenhouse cultures as a way of enriching the ambient air for better crop growth. The most popular method is using compressed industrial CO_2 which is vaporized into the greenhouse air. However, there are other methods, that each provide specific advantages, like a CO_2 generator where combustion of hydrocarbons produce CO_2 and simultaneously heat to warm the greenhouse, or having organic matter decompose within the greenhouse, which is a more environmentally friendly technique. Sublimation of dry ice and release of CO_2 by the chemical reaction of acetic acid and baking soda are other possible methods. [18]

All of these methods are responsible for producing and emitting CO_2 into the atmosphere because, as has been mentioned in chapter 1, the crops only take in about 10% of the provided CO_2, and the remaining 90% are released outside the greenhouse through ventilation.

Currently, in the Netherlands, some sustainable measures are already in place. The Shell oil refinery near Rotterdam has part of its emissions, which previously were released into the atmosphere, distributed by the Linde Group to about 580 greenhouses in the country, through a 300 km pipeline network. A smaller part of the CO_2 produced is liquefied in a purified state and sold to the food industry. The remaining emissions are intended to be captured and stored in empty natural gas fields off the coast of the Netherlands. [19] The Dutch waste recycling and waste to energy firm, AVR, in Duiven is seeking to do the same, having started the construction of a CO_2 capture process. [20]

Besides these large scale operations, some growers located next to a factory have a mutual beneficial relationship as is the case of an aubergine grower in Terneuzen, who has his greenhouses located 5 km away from an ammonia factory. The CO_2 produced in this factory is supplied to the crops and hot water from the factory is circulated through pipes for heating, successfully maintaining the temperature constant, while the cooled water flows back to the factory, in a cycle. [21]

Although these are commendable initiatives, still most of the CO_2 ends up in the atmosphere. The present assignment sought out to apply the DAC technology to the greenhouses, to capture the wasted CO_2 and provide it once more to the plants, either in pure form or in enriched air form. The sorbent selected for carbon capture by Veneman [14], can also be applied to DAC. The adsorption of CO_2 on Lewatit® VP OC 1065 has been extensively studied within the SPT research group, as well as several regeneration conditions, processes and several reactors and setup have been developed based on this sorbent. An overview of the relevant parameters and background to this assignment is described in the following sections.

2.6 Solid Amine Sorbent - Lewatit® VP OC 1065

Sorbent structure

The Lewatit® VP OC 1065 sorbent used in this research is a macroporous, divinylbenzene crosslinked polymer in spherical bead form with primary amine groups. Its structure is shown in the following figure.

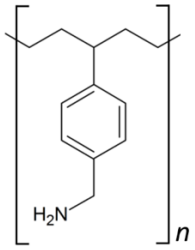

Figure 2.1: Molecular structure of Lewatit® VP OC 1065

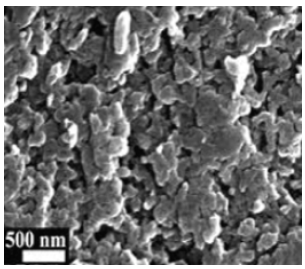

Figure 2.2: Surface of Lewatit® VP OC 1065 beads

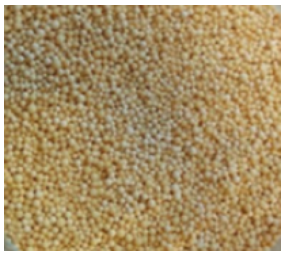

Figure 2.3: Lewatit® VP OC 1065 beads

CO_2 Adsorption

The primary amine functional groups are responsible for the selective adsorption of CO_2. The reaction mechanism of primary and secondary amines with CO_2 involves two steps. In the first one, CO_2 reacts directly with an amine molecule, forming a zwitterion. The zwitterion, in the second step, is deprotonated by a free base, either water or another amine, forming carbamate. Therefore, under dry conditions, one CO_2 molecule is captured by two amine groups. [14] The reaction pathway is the following.

$$RNH_2 + CO_2 \leftrightarrows RNH_2^+COO^- \tag{2.3}$$

$$RNH_2^+COO^- + RNH_2 \leftrightarrows [RNHCOO^-][RNH_3^+] \tag{2.4}$$

The extent of the reaction is limited by equilibrium. The amount of a compound that a sorbent can adsorb at a certain temperature is usually determined by isotherms. These isotherms are based on the thermodynamics of adsorption equilibrium and describe the influence of adsorbate concentration (or partial pressure P_i) and of the number of available adsorption sites n_s on the equilibrium sorbent loading q*. Several isotherm models have been developed, varying in complexity and applicability. Previous work [14] showed that the Toth isotherm model is the best fit for the experimental CO_2 adsorption data, and is described by the following equations.

$$q^* = \frac{n_s b P_{ads}}{(1 + (bP_{ads})^t)^{1/t}} \tag{2.5a}$$

$$b = b_0 exp\Big(\frac{\Delta H_r}{RT_0}\Big(\frac{T_0}{T} - 1\Big)\Big) \tag{2.5b}$$

$$t = t_0 + \alpha\Big(1 - \frac{T_0}{T}\Big) \tag{2.5c}$$

$$n_s = n_{s0} exp\Big(\chi\Big(1 - \frac{T}{T_0}\Big)\Big) \tag{2.5d}$$

Where q^* is the loading of the sorbent in mol_{CO_2}/kg_{sorb}, b is the equilibrium constant, t describes the heterogeneity of the adsorbent, ΔH_r is the isosteric heat of adsorption, R is the gas constant and T_0 is the reference temperature. The parameters α and χ determine the dependence of temperature relative to the

reference temperature T_0 for t and n_s, respectively. When considering chemisorption, the number of available sites is determined by the number of molecules on the adsorbent, which is independent of temperature. Therefore, χ is always equal to zero for chemisorption. [22] P_{ads} and T are the operation conditions of partial pressure of CO_2 and temperature, respectively.

The parameters, determined by M. Bos *et.al.*, used in this equilibrium model are present in Table 2.6 [1]. Figure 2.6 shows adsorption capacities determined by M. Bos *et.al.* using the equilibrium model, fitted to experimental results.

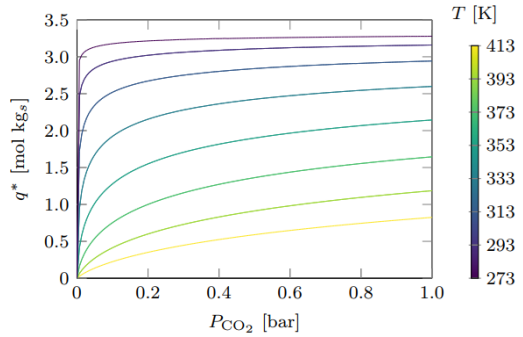

Figure 2.4: CO_2 adsorption isotherms for Lewatit® VP OC 1065 from 273 K to 413 K at 20 K intervals. The lines represent capacities calculated using the equilibrium model. [1]

Parameter	Value
t_0	0.37
b_0 (1/bar)	93.0
n_{s0} (mol/kg)	3.40
χ	0
α	0.33
ΔH (J/mol)	95.3$\times$ 10^3

Table 2.1: Toth isotherm parameters of the adsorption of CO_2 on Lewatit® VP OC 1065 using 353 K as reference temperature, as determined by M. Bos, *et. al.*. [1]

CO_2 Desorption

The reverse process of the adsorption is called the desorption. The desorption can either be performed to reduce the amount of adsorbed species so a new cycle of adsorption can start, or a regeneration step can be added, for full desorption and complete removal of the adsorbed species from the sorbent. This is used to regain full working capacity.

There are several methods for desorption, that can be classified in the following categories:

- **Pressure Swing Adsorption (PSA):** The adsorption is performed either at atmospheric pressure or at increased pressure. During desorption, the pressure is decreased below adsorption pressure, either to atmospheric pressure or using vacuum. Because the desorption process is endothermic, some heat can be provided. For final regeneration, an inert sweep gas can be added to purge the remaining CO_2.
- **Temperature Swing Adsorption (TSA):** Increased temperature reduces the equilibrium capacity of the sorbent, so desorption can be started by heating the sorbent, usually by heat transfer through flowing steam or hot water through a jacket around the sorbent bed or in pipes within the bed. A flow of electricity can also be used to heat up the sorbent. The expansion of gas because of its increase in temperature causes an effluent flow. For final regeneration, an inert sweep gas can be added to purge the remaining CO_2.
- **Concentration Swing Adsorption (CSA):** The inert sweep gas can be added when the desorption process starts, which reduces the partial pressure of CO_2 and acts as carrier. This is usually combined with heating to supply the heat of desorption.

These processes can be illustrated on the adsorption isotherm, the principles of PSA and TSA being represented in Figure 2.5, and the principle of CSA being similar to that of PSA. [22, 23]

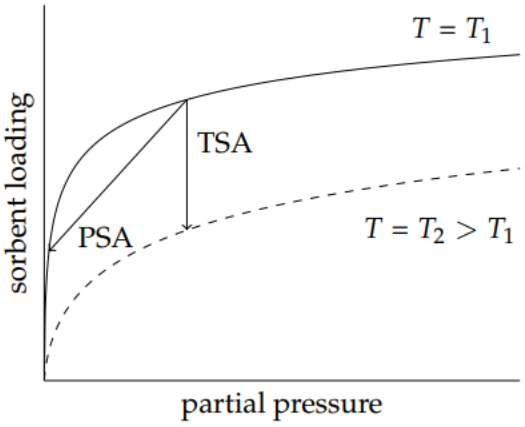

Figure 2.5: Illustration of temperature swing adsorption (TSA) and pressure swing adsorption (PSA), the arrows representing the respective desorption steps.

Often, the desorption process is performed under a combination of the described principles. Any combination of the three is likely to increase the working capacity of the sorbent and decrease the energy requirements per amount of CO_2 adsorbed. The inert species, or sweep gas used as purge are commonly either nitrogen, air, or steam. When using nitrogen or air, the product CO_2 is not pure, but rather a CO_2-enriched stream. If air is used as purge, the sorbent cannot be completely regenerated, because air contains CO_2 in an average concentration of 400 ppmV. When using steam, as it is easily condensable, a simple cooling treatment of the product stream can produce pure CO_2.

The working capacity of the sorbent depends on the adsorption and desorption conditions, which determine the CO_2 loading of the sorbent after each process. The difference between them is the working capacity (equation 2.6), which is an important parameter in process design.

$$\Delta q_w = q^*_{adsorption}(p,T) - q^*_{desorption}(p,T) \tag{2.6}$$

Effect of humidity on adsorption

It has been observed that the presence of water increases the CO_2 capacity of solid amine sorbents. Water molecules are non-competitively adsorbed onto the sorbent, according to the following reaction [24].

$$RNH_2 + CO_2 + H_2O \leftrightarrows RNH_3 + +HCO^{3-} \tag{2.7}$$

This results in a higher loading capacity for the sorbent, as water aids the adsorption. However, to increase the temperature for desorption and regeneration, the presence of water increases the energy requirements, as heat has to be provided to vaporize the water molecules adsorbed on the sorbent.

Sorbent degradation

The sorbent's stability is a very important factor in the viability of an adsorption process. If it is unstable and has to be replaced often, it can quickly become economically intensive, and can be restrictive on the conditions in which the reaction is processed.

Qian Yu,*et. al.*, showed that there was no loss of capacity of the sorbent when exposed to temperatures up to 150°C in nitrogen. At 200°C there was some observable thermal degradation, with 39% capacity loss after 50h of exposure [15]. However, when compared to other sorbents, namely those impregnated with amines instead of bound to, the Lewatit particles show great thermal stability [14].

The stability in CO_2 was also studied. In the presence of CO_2, degradation occurs already at lower temperatures. If the partial pressure of CO_2 approaches 1 bar, the maximum temperature should not be higher than 120°C so as to avoid the formation of urea [15]. In the presence of oxygen, the degradation is more significant already at temperatures above 70°C [15].

Qian Yu, *et. al.*, also showed that there is no difference in stability between continuous and cyclic treatment, and therefore the cyclic adsorption-desorption has no effect on sorbent degradation [14].

2.7 Reactor design

Reactor types

Three different reactor types where considered for this application of DAC technology: fixed bed axial flow, fixed bed radial flow and fluidized bed reactors. The difference between the reactors is based on different gas-solid contact modes. In both fixed bed reactors the solid sorbent is immobilized as the gas flows through the bed. On the other hand, in a fluidized bed the gas stream fluidizes the solid layer, increasing its porosity and bed height. A representation of the contactor types can be seen in Figure 2.6.

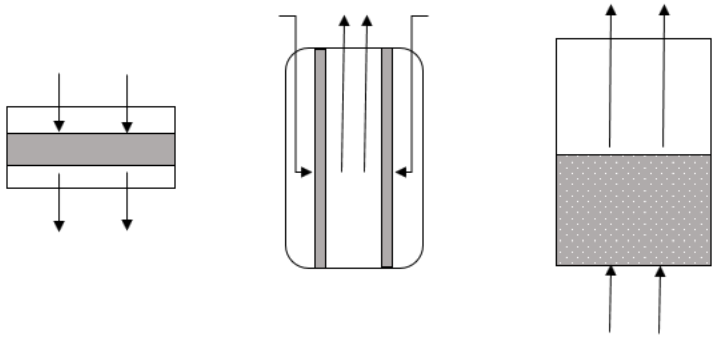

Figure 2.6: Side view of the types of reactors considered in this thesis. Arrows mark the direction of the gas flow

Fixed Bed Axial Flow Reactor

Fixed bed reactors with axial flow are widely used in the industry, as they are easy to design and operate. Other advantages include ideal plug flow behaviour, lower maintenance costs and reduced loss due to attrition and wear. In the design of a fixed bed reactor, heat transfer and distribution are important parameters, as poor heat transfer may result in generation of hot spots and thermal degradation and poor heat distribution may lead to non uniform reaction rates and, therefore, reduced conversion. This becomes a bigger issue in large beds and highly temperature dependent reactions. Disadvantages of fixed bed reactors include the difficulty in regenerating or replacing the sorbent, high pressure drops observed for small beads, and sometimes attachment of the beads to each other and to the vessel, which also results in high pressure drops. [25]

The pressure drop (ΔP) in fixed beds can be calculated by the Ergun equation (equation 2.8), where L_m is the length or thickness of the bed, g_c the correction factor, ε_m is the porosity of the bed, or its void fraction, μ is the viscosity of the gas flow, u_0 is its superficial velocity, d_p is the particle diameter, ϕ_s is the sphericity of the particles, in this case assumed to be 1, and ρ_g is the particle's densitity. [26]

$$\frac{\Delta p}{L_m} g_c = 150 \frac{(1-\varepsilon_m)^2}{\varepsilon_m^3} \frac{\mu u_0}{(\phi_s d_p)^2} + 1.75 \frac{1-\varepsilon_m}{\varepsilon_m^3} \frac{\rho_g u_0^2}{\phi_s d_p} \tag{2.8}$$

Fixed Bed Radial Flow Reactor

Radial flow reactors, when compared to axial flow reactors, have the advantage of allowing a bigger surface area in the same occupied space, therefore permitting a thinner layer, thus, a lower pressure drop. [27] The design of a radial flow reactor is more complicated than that of an axial flow reactor; its main issues are flow distribution along the length of the reactor, thermal reaction in the void space and expansion and contraction of the catalyst basket. Radial flow reactors are appropriate for large scale processes, as axial reactors require an increase in diameter so as not to increase the pressure drop beyond feasible values, and large diameters are not practical. In contrast, radial flow reactors can be scaled up in height instead of diameter, which is advantageous. Since in a radial flow reactor the gas stream is fed along the length of the reactor, there is a larger cross-sectional area available for the flow and the sorbent bed can be shallower, which results in the lower pressure drop. [28]

Fluidized Bed Reactor

In a fluidized bed reactor, the solid sorbent is fluidized by the gas stream. The linear velocity of the gas stream is kept above the minimum fluidization velocity (u_{mf}), otherwise the bed will behave as a fixed bed. Minimum fluidization occurs when the pressure drop (ΔP) over the bed equals the weight of the particles, and is determined experimentally.

$$\Delta P = (\rho_p - \rho_g)(1 - \varepsilon_{mf})g.L_{mf} \tag{2.9}$$

Where ρ_p is the particle density, ρ_g is the gas density, ε_{mf} is the bed porosity at minimum fluidization, g is the gravity force and L_{mf} is the bed length or thickness at minimum fluidization.

The higher the superficial velocity of the gas stream, the more the bed expands. When the superficial velocity equals the terminal velocity of the particles, these escape the reactor. [25]

At superficial velocities above minimum fluidization velocity, the pressure drop is close to constant [26]. Therefore, the pressure drop depends only on the bed height at minimum fluidzation, which is determined by the following equantion 2.10. Driessen, *et. al.*, determined the minimum fluidization velocity and bed porosity at minimum fluidization of Lewatit VP OC 1065 experimentally, as 0.091 m/s and 0.51, respectively [2].

$$L_{mf} = \frac{V_{sorbent}}{(1 - \varepsilon_{mf})A} \tag{2.10}$$

$V_{sorbent}$ being the volume of sorbent in the bed, and A the surface area of the bed.

Driessen, *et. al.*, on studying a multistage fluidized bed using the same sorbent to remove CO_2 from sour gases, concluded that on the basis of the physical properties of the amine sorbent, it can be classified according to Geldart's classification for fluidization as Geldart B (sand-like) powder. [26, 29] For a Geldart B (sand-like) powder, bubbles will form as soon as the minimum fluidization velocity is reached, and small bubbles formed just above the gas distributor will grow while upflowing along the fluidized bed. These bubbles induce solid circulation and thereby mixing of the fluidized bed. Furthermore, when fluidizing the sorbent particles, fluidization will be in the bubbling regime for appropriate superficial gas velocities, which is common for Geldart B powders. Driessen, *et. al.*, visually confirmed this by fluidizing the amine sorbent in a glass column [29].

Compared to a packed bed, heat transfer is more efficient in a fluidized bed, resulting in a more uniform temperature in the reactor. Another advantage is that regeneration of the sorbent can be done without shutdown of the process. However, this type of reactor is a complicated system to operate and requires higher operating and maintenance costs, as well as extensive investments due to the moving solids. Attrition and

sorbent loss due to fluidization and circulation can also be an issue. [25]

2.8 Design basis

For low costs of CO_2 adsorption from the air in the greenhouse, the performance of the gas-solid contactor is important. This depends on feed conditions, reactor dimensions and operating conditions. One relevant performance indicator is the adsorption rate, meaning, the time it takes to achieve a certain loading of CO_2 on the sorbent. This rate determines the number of cycles that can be run per day, and is specific to the type and dimensions of the contactor. The adsorption rate can be determined experimentally through the breakthrough curve, and this has been done for ambient air and different concentrations of CO_2 by several studies within SPT [14, 15, 30]. The adsorption time can be compared to the stoichiometric adsorption time, which is the minimum time it would take to achieve a certain level of CO_2 loading on the sorbent. In other words, it is the time it would take to reach equilibrium loading if the CO_2 adsorption was instant and complete. The stoichiometric time (t_{stoich}) at 100% loading can be calculated with the ratio between the CO_2 loading and the amount of CO_2 in the feed. This is described in equation 2.11, where m_s is the mass of sorbent in the bed, q^* is the equilibrium loading φ_v is the feed flow rate and C_{CO_2} is the concentration of CO_2 in the feed.

$$t_{stoich} = \frac{CO_2 capacity(mol)}{CO_2 feed(mol/s)} = \frac{m_s q_e}{\varphi_v C_{CO_2}} \tag{2.11}$$

In order to evaluate the energy intensity of each type of contactor, the energy calculations required for the process were performed.

First, the sensible heat to be transferred to the sorbent, $Q_{sensiblesorbent}$ is calculated using equation 2.12, using the temperature difference between the adsorption and the desorption.

$$Q_{sensiblesorbent} = m_s.C_{p,s}(T_{desorption} - T_{adsorption}) \tag{2.12}$$

$C_{p,s}$ is the heat capacity of the sorbent and T is the temperature. The sorbent mass, m_s, is calculated by the amount of dry sorbent needed to capture 1 kg of CO_2 using the working capacity, Δq_w, in the working conditions. MW_{CO_2} is the molecular weight of CO_2.

$$m_s = \frac{1}{\Delta q_w.MW_{CO_2}} \tag{2.13}$$

As the desorption reaction of the CO_2 from the sorbent is endothermic, energy supply is necessary to release the CO_2 from the amine. The amount of energy required, per kilogram of CO_2, is calculated from the reaction heat, with equation 2.14.

$$Q_{reactionheat} = \frac{\Delta H_r}{MW_{CO_2}} \tag{2.14}$$

As the sensible heat taken up by the CO_2 is determined by equation 2.15, where C_{p,CO_2} is the heat capacity of CO_2.

$$Q_{sensibleCO_2} = C_{p,CO_2}(T_{desorption} - T_{adsorption}) \tag{2.15}$$

To reduce the pressure inside the reactor and overcome the pressure drop from the flow rate through the sorbent particles, energy is required to compress the air. Adiabatic compression is assumed, and calculated by

equation 2.16.

$$Q_{aircompression} = \frac{1}{\eta}.\frac{k}{k-1}.\phi_{mole,CO_2}\Big(1+\frac{1}{ratio(CO_2/purge)}\Big).RT\Big[\Big(\frac{p_2}{p_1}\Big)^{k-1/k}-1\Big].t \tag{2.16}$$

The efficiency of the compression, η, is assumed to be 0.75, and the ratio of Cp/Cv, k, is 1.3 for air [31]. ϕ_{mole,CO_2} is the molar flow of CO_2, $ratio(CO_2/purge)$ is the molar ratio of CO_2 in the total gas flow, R is the gas constant and T is the temperature at which the operation is preformed. In the case of gas compression to overcome pressure drop, p_2 is $\Delta P + p_{atm}$ and $p_1 = p_{atm}$ is assumed to be 1 bar and t is either the time of the adsorption or the time of the desorption.

3 Reactor Design

In this chapter, the goals and process parameters of the to-be-designed installation are discussed, along with preliminary and simplified designs and calculations of the three types of rector described in chapter 2. The purpose is to determine which type of reactor is more favourable for an installation of this scale, and to determine its operation conditions.

3.1 Process Parameters and Selection of Reactor Type

The greenhouse of Royal Roses, for which the installation is to be designed, is a 3 hectare culture of red roses, planted in rows of 200 m^2. For year round culture, pure industrial CO_2 is supplied to the plants. In winter, approximately 30 ton of CO_2 are provided per week while, in summer, this value rises to 180 ton per week. From this amount, only an average of 10% is taken in by the plants for their growth, while the other 90% are being wasted into the air of the greenhouse and ultimately into the atmosphere. The goal is to design an installation that can capture part of the wasted CO_2 from the ambient air inside the greenhouse, above crop level, and supply it again to the plants at leaf height, in a concentrated form. For this, a basis of design of 1 row of plants of 200 m^2 was used as goal, which requires about 28 kg of CO_2 per day, in winter. Aiming for a 50% reduction of the supplied industrial CO_2, the design basis is an installation that can provide 1 kg/h of CO_2 continuously, working 14h per day, approximately during the time when the culture actually does photosynthesis, in the form of 1% v/v CO_2-enriched air.

For the initial calculations, with the purpose of defining the type of reactor which best suits the requirements, some approximations and assumptions were made. Firstly, the effect of water in the air was dismissed in the calculation of the working capacity of the sorbent. Secondly, a constant inlet concentration of 600 ppm of CO_2 was assumed, as this is the average concentration around the top of the plants. Thirdly, an adsorption time of 1 hour was considered and, based on the breakthrough curve obtained by Natalia Frigka [30], a sorbent efficiency of 75% was assumed.

Based on these assumptions, the working capacity can be calculated with the isotherm described by equations 2.5a to 2.5d in chapter 2 for adsorption at 21°C (the temperature at which the greenhouse is kept) and 600 ppm concentration in the feed air, and a desorption with air at 70°C, the maximum temperature at which the desorption can be performed in the presence of oxygen. In these conditions, with a sorbent efficiency of 75% in the adsorption, the working capacity is 0.8 mol/kg. For 1 kg of CO_2, about 30 kg of sorbent and 2.7×10^3 m^3/h of 600 ppm air are required. In the desorption process, to achieve a 1% v/v concentration of CO_2 in the product stream, 55 m^3/h of purge air is necessary. With these values, drafts of the three different types of contactors described in chapter 2 can be obtained.

For the fixed bed, both axial and radial, the pressure drop along the bed increases the thicker the bed. An increase in pressure drop means an increase in the necessary compression power of the air stream to overcome the given pressure drop, thus higher operation costs. Therefore, it is important to know what the weight of this factor is on the overall costs. For this, the energy demand calculations described in chapter 2 were done for different bed heights, in the range of 0.5 cm and 10 cm. However, with a fixed amount of sorbent and air flow rate, the diameter of the axial fixed bed is smaller when the bed is thicker and, thus, the superficial velocity is higher, which further increases the pressure drop. This being the only criteria, the reactor should be as shallow as possible. However, this would increase the footprint of the bed a lot, which is not practical above a certain limit value of diameter. In the radial flow fixed bed, the same bed heights were tested, keeping

the inner diameter of the cylindrical bed constant, at 30 cm. The difference in bed thickness leads, then, to a taller or shorter bed. A thicker bed means a shorter reactor, thus a smaller superficial area, therefore a higher superficial velocity of the air, but the increase in pressure drop is the same as in the axial fixed bed. The results of this sensitivity analysis are shown in Figure 3.1 and more detailed calculations and results can be consulted in appendix A.4.

As for the fluidized bed contactor, at superficial velocities above the minimum fluidization value the pressure drop remains constant. However, the pressure drop does change with the height of the bed at minimum fluidization velocity. So, by increasing the bed height the pressure drop does increase, and so does the energy demand for compression of the air stream, but this increase is quite less marked than in a fixed bed. This because the pressure drop in a fluidized bed increases linearly with the bed height, and the pressure drop in a fixed bed increases both linearly with the bed height and with the superficial velocity of the air, in the first term linearly, and in the second term quadratically.

Because the sensible heat transferred to the sorbent, CO_2, and the heat of reaction are independent of the contactor design, only the compression energy in the adsorption and desorption steps is relevant for this sensitivity analysis. This is shown in the Figure 3.1. Because, in the fluidized bed design, the desorption flow rate does not allow minimum fluidization, during desorption the bed must act as a fixed bed and the pressure drop and compression energy are equal in both types of contactors.

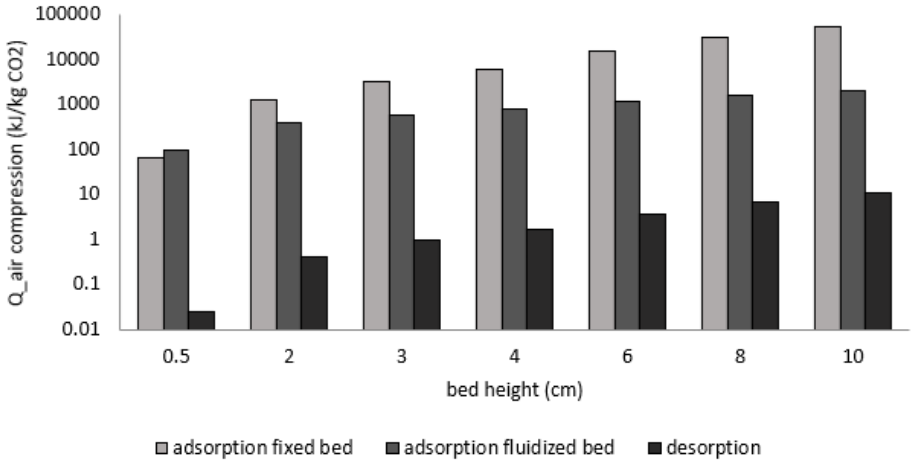

Figure 3.1: Air compression energy required for adsorption and desorption in fixed and fluidized beds as function of the bed height, for constant amount of sorbent (30 kg), ambient air flow rate, 2.7×10^3 m^3/h, and flow rate of purge air in the desorption, 55 m^3/h. Compression energy in logarithmic scale.

In the fixed bed, the compression costs of the air in the adsorption stage increase significantly with the increase of bed height, from 68 MJ/kg of CO_2 at 0.5 cm height, to almost 55×10^3 MJ/kg in a 10 cm tall bed. In the fluidized bed, the increase is still significant, from 98 to almost 2000 MJ/kg of CO_2, but the increase is linear with the bed height. A shallow bed is, thus, advantageous.

Despite this analysis, when defining design parameters, low costs of air compression are not the sole criteria. A trade-off of costs and efficiency and reasonable dimensions needs to be found. For instance, to have the lowest possible costs of air compression, the 0.5 cm tall bed should be chosen, regardless of the type of reactor. However, this bed would be 3.7 m in diameter, which is not reasonable, or need to be divided in many units, which ends up increasing production, maintenance and operation costs. As these designs do not yet go into the intrinsic dynamics of the system, to narrow the option down to one type of contactor, very simplified estimates were made of each type. For comparison between the three types, axial flow fixed bed, radial flow fixed bed, and fluidized bed, the first three estimates were made with the same bed thickness, shown in Table

3.1. Secondly, three estimates with similar pressure drop along the bed were compared, shown in Table 3.2. The values for superficial velocity and pressure drop are for the adsorption process because this represents a bigger contribution to the air compression costs than the desorption, as can be seen in Figure 3.1.

Table 3.1: Dimensions, superficial velocity of the air during adsorption and pressure drop along the bed of the different possible types of contactors for similar bed thicknesses. The bed thickness of the fluidized bed is the correspondent fixed bed height, so, the bed height at conditions below minimum fluidization.

	Fixed bed	Radial flow	Fluidized bed
L (cm)	3	3	3
Diameter/Height (m)	1.49	0.3/1.85	1.49
u_0 (m/s)	0.44	0.44	0.44
Δp (Pa)	873	873	162

Table 3.2: Dimensions, superficial velocity of the air during adsorption and pressure drop along the bed of the different possible types of contactors for similar pressure drops. The bed height of the fluidized bed is the correspondent fixed bed height, so, the bed height at conditions below minimum fluidization.

	Fixed bed	Radial flow	Fluidized bed
L (cm)	2	2	6
Diameter/Height (m)	1.82	0.3/2.77	1.05
u_0 (m/s)	0.29	0.29	0.87
Δp (Pa)	353	353	323

From the estimates on Table 3.1 it can be seen that, given the same bed thickness and superficial velocity, the pressure drop of the fluidized bed is far below the pressure drop on both fixed beds. The air compression costs are lower then. On the other hand, with a similar pressure drop, therefore, similar air compression costs, the design for the fluidized bed is more space efficient, occupying a smaller area.

Between the two types of fixed bed, the radial flow reactor is, of course, a lot more space efficient than the axial flow one, but at the same conditions they have the same costs. The height of the column of the radial flow reactor is also important though, because the taller the bed, the more uneven the flow distribution in the bed is (the same applies for wide beds). Besides, as the installation is for inside a greenhouse, it must fit inside the smaller greenhouses, which are 3 meters in height.

So, two initial estimates were chosen: the radial flow reactor with a bed thickness of 3 cm and 1.85 meters high column and the fluidized bed with 6 cm of bed thickness (when not fluidized) and 1.05 m of diameter. For these designs, the energy demand values in Figure 3.2 were determined.

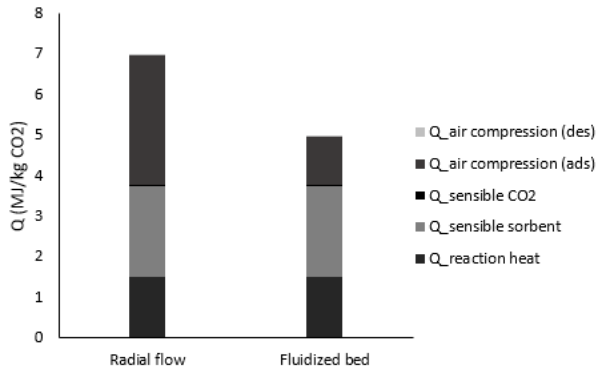

Figure 3.2: Energy demand estimates of the two different reactors considered.

The fixed bed radial flow reactor, even though it has higher energy demands than the fluidized bed, still has advantages to it, that can prove to outweigh the disadvantage of the higher energy demand. Therefore, this option can not yet be discarded, and for a more detailed comparison between the fluidized bed and the fixed bed the advantages and disadvantages of each should be weighted.

In a fixed bed, there is more contact between the two phases, solid and gas, because the air flow is determined by the space between the sorbent particles. However, in a fixed bed, only the sorbent layer on the inlet air side is contacted with new air. The further along the bed the air flows, the less CO_2 it transports. So, the sorbent bed is loaded slowly along its thickness, creating a gradient of CO_2 loading. The top layer of sorbent takes a long time to become fully adsorbed because, initially, it contacts mostly CO_2 stripped air. In a fluidized bed, the sorbent in the bed is mixed over time, so there is no loading distribution or gradient within the bed, which results in a more efficient contact between gas phase and solid phase. Therefore in a short adsorption time, a fluidized bed allows a higher overall sorbent loading than a fixed bed.

If the adsorption is more efficient, the working capacity of the process increases and, thus, less sorbent is needed. A smaller volume of sorbent means a smaller footprint of the reactor, and, because the bed is fluidized and this allows a lower pressure drop, the bed can be thicker and more narrow than the fixed bed, which further optimizes space.

Furthermore, unlike the fixed bed, the fluidized bed does not necessarily require the adsorption and the desorption to be performed in the same equipment. This is beneficial, in this case, because, with the dimensions designed for the adsorption, the flow rate used in the desorption does not allow high enough a superficial velocity for bed fluidization. Therefore, the desorption can be done in another reactor, and, as a consequence, there is a need for sorbent circulation. Sorbent circulation implies more maintenance required and possibly more frequent sorbent replacement due to its faster degradation. Sorbent circulation allows, on the other hand, a continuous throughput of CO_2 enriched air, which non circulating sorbent (like in a fixed bed) does not. For a fixed bed to be able to produce a steady output of CO_2 enriched air, a duplicate is necessary, which runs in alternate cycles. Having a duplicate implies twice as much sorbent, which poses a disadvantage of this mode of operation. To be more space effective, instead of 2 very large units, 4 smaller units can be stacked on each other, and all run in alternate cycles, which allows an output of CO_2 enriched air which is close to continuous. Fixed beds are more compact and robust, because they lack the moving solids, thus the necessary maintenance is minimized, which, in principle, reduces the operation costs.

Because the sorbent is moving within the bed, a fluidized bed is more efficient in heat transfer than a fixed bed. Due to the circulation of sorbent in the bed, heated and cold sorbent particles are mixed and temperature is homogenized, not allowing the formation of a heat gradient and therefore no hotspots or cold areas, which will be the case in a fixed bed. As there is better heat distribution, also the desorption process will be more efficient, because it takes less time for the bed to reach desorption temperature.

The advantages and disadvantages of fixed and fluidized beds as described are summarized and compared in the following Table 3.3.

Table 3.3: Pros (green dots) and cons (red dots) of fluidized bed reactor versus fixed bed reactor

Fluidized bed	Fixed bed
2 units (adsorber+desorber) 🔴	1 unit 🟢
Single sorbent inventory 🟢	Duplicate sorbent inventory 🔴
Circulating sorbent 🟢 🔴	Fixed sorbent 🟢 🔴
Less heat transfer limitations 🟢	More heat transfer limitations 🔴
More maintenance required 🔴	Less maintenance costs 🟢
More fragile installation 🔴	More compact and robust 🟢

Even though a fluidized bed has a more fragile structure than the fixed bed and is likely to require more maintenance over time, the advantages do outweigh the disadvantages. Also, the maintenance requirements of the setup is not a given truth. The more complex heating system of the fixed bed can, ultimately, tip the scales. As for the sorbent maintenance, the fluidized bed requires a lot less sorbent than the fixed bed, so even if it needs to be replaced more frequently, it can still be the more economic solution. It also allows a continuous output of CO_2, which, for the application it is intended, is the goal. Besides these reasons, the adsorption process is more efficient, due to the lack of a loading gradient in the bed. This analysis makes the fluidized bed a better choice for this application.

3.2 Fluidized Bed Design

To produce 1 kg/h of CO_2, a large volume of greenhouse air needs to be treated (for an approximate capture efficiency of 50%, flow rates of 1500 to 2700 m^3/h need to circulate through the system, depending on the CO_2 concentration (400-800 ppm) in the air). In fluidized beds, increasing superficial velocities above minimum fluidization increases the bubble phase and the flow becomes turbulent. As a result, channelling occurs and the contact between air and solid decreases, decreasing mass transfer efficiency. The channelling effect also increases due to bubble formation when the bed is wider and higher, as the size of the bubbles increases between the moment they are formed at the distributor and the top of the bed. This can be an issue when scaling up. However, if the height (bed thickness) remains low, the effect of bubble size increase is likely to be low. [29]

Lower superficial velocities have also proven to result in lower outlet gas concentrations (when working in continuous mode) and higher tray efficiencies (when working in multistage setup) [29]. With lower superficial velocities, the gas residence time is higher, allowing more time for the CO_2 to be adsorbed onto the sorbent and reaching equilibrium loading. However, with higher superficial velocities the amount of CO_2 inserted in the system is bigger, thus the sorbent gets into contact with bigger quantities of CO_2 in the same time. Therefore, a trade-off must be found, a high enough superficial velocity that maximizes the amount of CO_2 inlet, and optimizes the residence time and contact with the sorbent, without increasing the channelling effect. This trade-off of superficial velocities must also be combined with the trade-off of bed heights, as a shallow bed decreases bubble size and therefore bypassing, but a bigger bed height increases the residence time of the air.

For flow rates of 1500 to 2700 m^3/h to flow through shallow beds at a low superficial velocities, a big surface area is necessary. In a single vessel, the diameter of the adsorption bed would have to be from 1 to 2.5 m to keep the mentioned flow rates at a low superficial velocity (under 0.5 m/s). Meanwhile, the desorption requires a flow rate of 55 m^3/h to produce enriched air of 1% CO_2. For low superficial velocities (0.09 - 0.15 m/s), the required desorption bed diameter is 40 cm. This is a more reasonable dimension, and as in practical terms it is easier if the adsorber and the desorber have the same dimensions, the adsorber can be divided in several stages of 40 cm diameter each, and the inlet gas stream is divided between the different stages. These different stages can be stacked up on top of each other, much like a multistage fluidized bed, where the lean sorbent enters at the top stage and flows down, from stage to stage, until it leaves the bottom stage loaded with CO_2. However, unlike a counter current multistage fluidized bed where the air enters in the bottom stage through a distribution plate and passes all the stages until it leaves the top, each stage has an air inlet and outlet, therefore, the sorbent in each stage is contacted with new air. The design of one of these cross flow adsorption stages is shown in Figure 3.3.

From the bottom stage of the adsorber, the sorbent will fall into the desorber, that, for increased efficiency, has several stages in the counter current layout: air inlet in the bottom, air outlet at the top, flowing through all the stages. The desorption can done with air as purging fluid, because it is available at no additional investment cost, as opposed to pure nitrogen or steam. This means, however, that the desorption will be

performed in the presence of oxygen, thus cannot be operated at temperatures above 70°C, otherwise the degradation of the sorbent is significant [15].

The heating of the stages in the desorber can be done by heat transfer across the cylinder wall of each stage, but, as the diameter is considerable and it would be difficult to have the temperature radially homogeneous, also the perforated plates on which the sorbent rests could be heated. By contact with the warm plates, the air will increase in temperature as well and contribute to the heating of the sorbent. The fluidization itself induces mixing and homogenization of the bed, providing better heat transfer. In a study on axial dispersion, J. Linden showed that, by pouring hot sorbent onto a cool fluidized bed, the temperature was vertically homogenized within a few seconds (for a bed height of 170mm and u_0=1.52u_{mf}, in 20 seconds the temperature was homogeneous along the axis of the bed) [32]. This shows a fast temperature homogenization within the bed. A representation of a desorption stage is shown in Figure 3.4.

The lean sorbent, at 70°C, leaves the bottom of the desorber, its flux controlled by a rotary valve, and is conveyed into a riser. The riser has a flow of ambient air that pneumatically transports the sorbent to the top of the adsorber, while it is cooled with cold water flowing in a jacked lining the wall, and by the cool air itself. At the top of the riser a cyclone separates air from the sorbent, and the lean sorbent enters the top stage of the adsorber once more. The sorbent is, however, not entirely lean. As the desorption is performed with air, which contains CO_2, the sorbent will leave the desorber at the equilibrium loading at these conditions (400ppm and 70°C), 0.21 mol/kg, value obtained from the Toth isotherm seen in chapter 2. In the riser the sorbent comes into contact, again, with air, and as it is at a lower temperature some CO_2 may be adsorbed as well. However, the extent of this adsorption is hard to quantify, but as the contact time is very low, it is assumed that the sorbent enters the adsorber with a loading of 0.21 mol/kg. The first draft of a design of the full reactor is displayed in Figure 3.5.

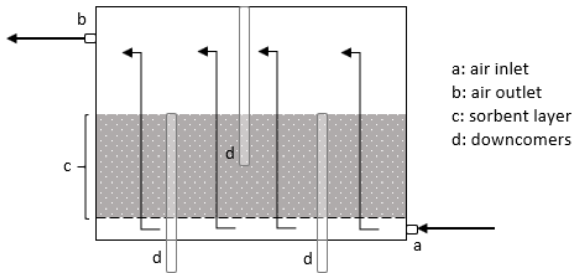

Figure 3.3: Design of an adsorption stage

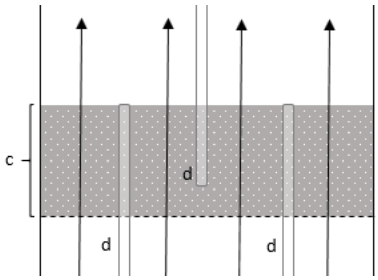

Figure 3.4: Design of a desorption stage

The exact dimensions and number of stages, both in the adsorber and the desorber, as well as the superficial gas velocity and sorbent flux, can not be defined as of yet. To do so, experimental data is necessary, to determine which design parameters and operation conditions can provide the desired output of 1 kg/h of CO_2, at a relatively low cost. This experimental data was obtained using a setup and procedures described in chapter 4.

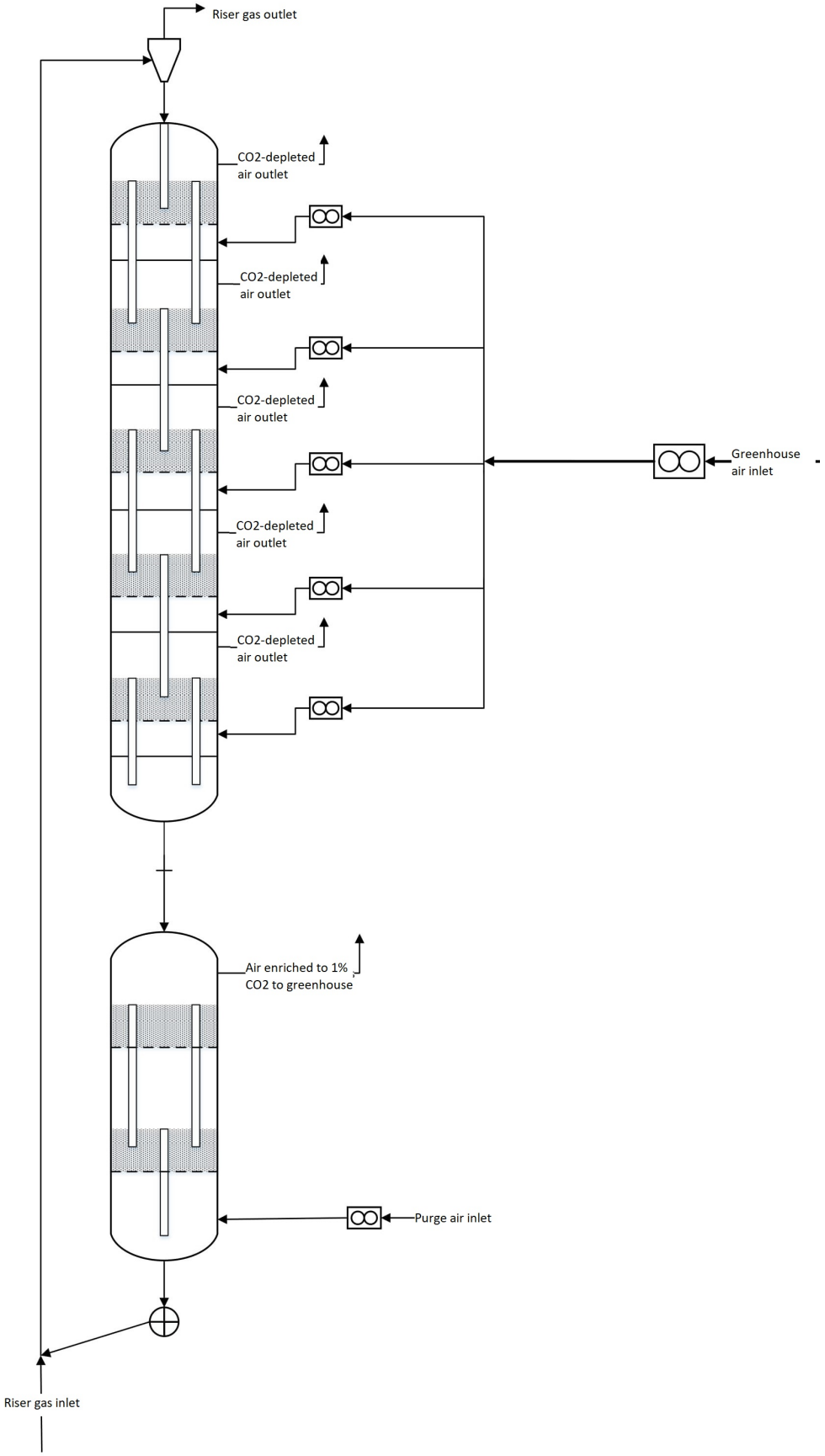

Figure 3.5: Design of the reactor

4 Experimental

4.1 Fluidized Bed Setup

For the experimental part of this assignment, a multi-stage fluidized bed (MSFB) setup was used. The setup is comprised of an adsorber, a desorber and a riser, which allows sorbent circulation. The setup can be seen on Figure 4.1.

The adsorption column is constructed in modules, which can be added or removed in order to increase or decrease the number of stages. There are five stages in total. Each module is 15 cm tall and has a 10 cm internal diameter, and can be stacked on top of each other and held air-tightly together by flanges. One stage is made of two modules, with a perforated plate (triangular pitch of round holes, 0.5 mm hole diameter, 1.5 mm hole pitch) on the bottom one, and two standpipes (13 mm internal diameter) which allow the sorbent to overflow to the next stage. The height of the standpipes above the perforated plate can be adjusted to vary the bed height. At the lowest stage, a metal sintered plate is installed instead of a perforated plate to ensure an even initial distribution of gas. Each stage was fitted with a sample point in the freeboard, connected to a LI-COR LI-840A CO_2 analyzer (calibration range: 0 - 10 000 mol ppm CO_2). Besides this, K-type thermocouples were installed at each stage 20 mm above the distributor, as well as at the gas inlet to the adsorber. Figure 4.1 shows the overview of the setup and the internals of the adsorber in more detail.

The desorber is a five stage fluidized bed, with internal diameter 10 cm. In the desorber, the number of stages cannot be changed. Each stage is equipped with heat tracing, in order to heat up the stages to desorption temperature ($\sim$110°C). These stages are also defined by perforated plates with standpipes to allow the overflow of sorbent to the following stage. The bottom stage is connected to a rotary valve which regulates the sorbent flux into the riser. The sorbent rises by a flow of nitrogen, while it is cooled by water on the outside.

The gas flow in any part of the setup is controlled by mass flow controllers (MFCs). The nitrogen flow to the adsorber is controlled by two MFCs: a Brooks Instrument 5851 MFC (0-70 L min^{-1}) and a Brooks Instrument 5851E MFC (0-100 L min^{-1}). The CO_2 flow is controlled by a Brooks Instrument MFC (0-150 mL min^{-1}). These three inlet flows are mixed before entering the adsorber. The riser gas flow is controlled with a Brooks Instrument 5850 MFC (0-11 L min^{-1}). The gas flow to the desorber is regulated by a Brooks Instrument 5851S MFC (0-100 L min^{-1}). All MFCs were carefully calibrated using appropriate gas flow measuring devices.

In both the adsorber and the desorber, the gas inlet is at the bottom stage, and is contacted with each stage until flowing out at the top. The sorbent flows in at the top of the column and leaves at the bottom. The sorbent is fluidized by the gas flow, with the overflow falling through the standpipes into the stage bellow. From the bottom stage of the adsorber, the overflow of sorbent goes into the desorber, its flux being regulated by a rotary valve. In the desorber, the sorbent is stripped of its CO_2 content by a nitrogen purge. The resulting flue gas exits the column at the top. At the bottom of the desorber, a rotary valve determines the solid flux to the riser. The riser is a long, thin tube (8.5 mm internal diameter) with a cooling jacket around it that connects the bottom of the desorber with the top of the adsorber. The sorbent is transported by a nitrogen flow to the top of the adsorber at a superficial velocity of $\sim$3.5 m/s, where a cyclone separates the sorbent from the nitrogen flow and the fines. The lean sorbent then enters the top of the adsorber again.

The experiments performed in this report were executed with a single stage adsorber, meaning, the remaining four stages were removed. The breakthrough curves of adsorption were obtained from performing the

adsorption in a single stage, without circulation of the sorbent. The regeneration between experiments was done at ∼110°C with circulation.

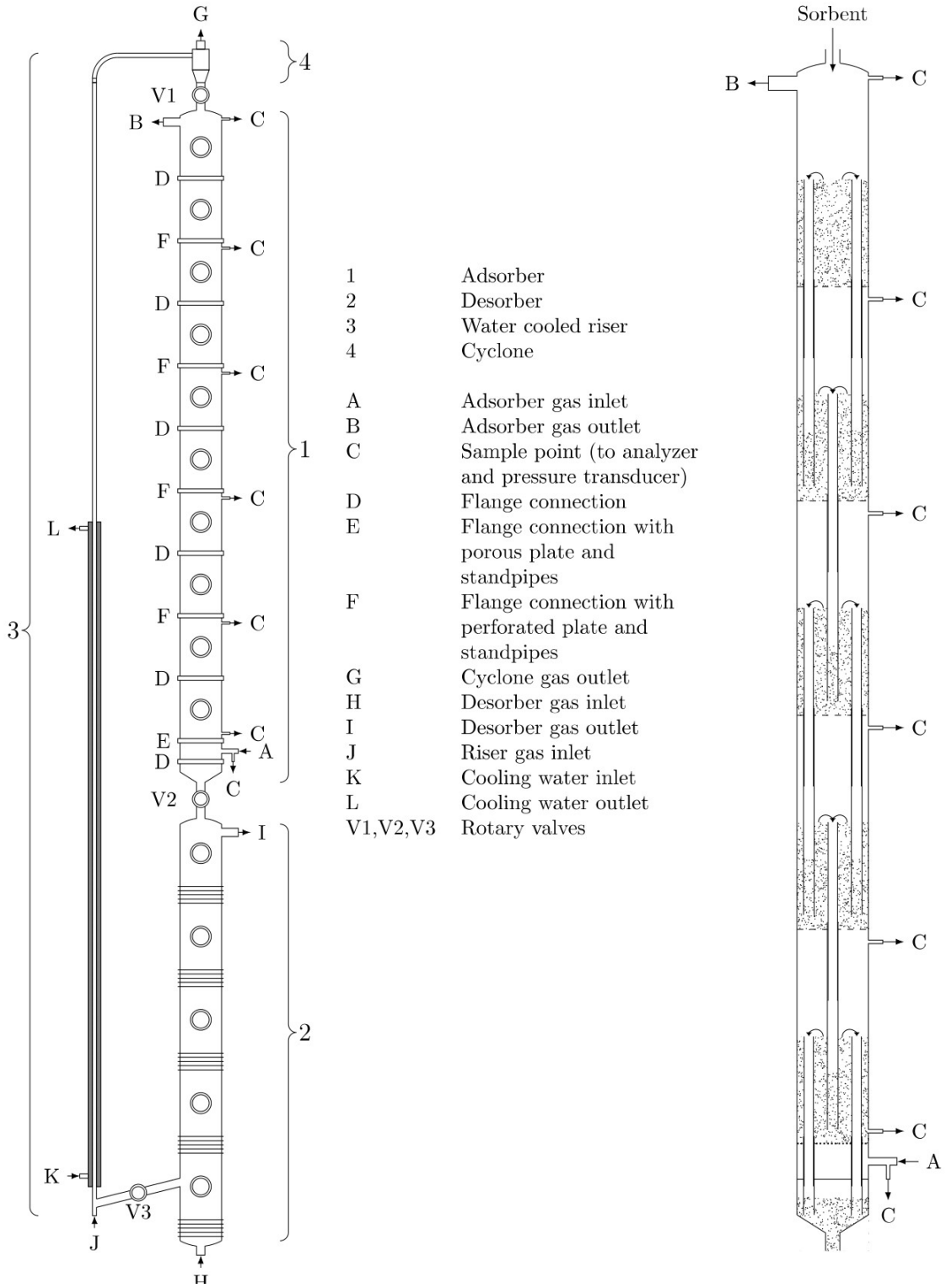

Figure 4.1: Schematic overview of the multistage fluidized bed setup, and cross-sectional view of the interior of the adsorber [2]

4.2 TGA

The Thermogravimetric analysis (TGA) was used as a supporting method to determine the capacity of the Lewatit® VP OC 1065. I was used both for samples of fresh sorbent and for samples of the sorbent in the fluidized bed setup, in order to compare the measured capacity with the equilibrium loading given by the isotherm described in chapter 2. It was performed in a Netzsch STA 449 F3 Jupiter® using aluminum oxide crucibles.

Figure 4.2 shows a typical result of a TGA measurement. At first, the sample (of about 10 to 15 mg) is heated to 120°C under a flow of 100mL/min of pure nitrogen. Once at this temperature, these conditions are maintained for 3 hours, to fully desorb all CO_2 and water that is on the sorbent. After the desorption, the temperature is lowered to 40°C. At this temperature, the flow alternates to a 15 vol% CO_2/N_2 mixture. The temperature and flow are maintained for 3 hours until complete adsorption of the sample. The mass variations of the sample are measured over the whole time of the analysis. Any mass change effects due to the crucibles and sample holder are eliminated with a correction file for the crucibles alone. The capacity of the sorbent is determined equation 4.1, where $m_{desorbed}$ is the mass of the fully desorbed sample and m_{diff} is the difference in mass between the fully desorbed sample and the loaded sample. m_{diff} is the mass of CO_2 adsorbed on the sorbent sample.

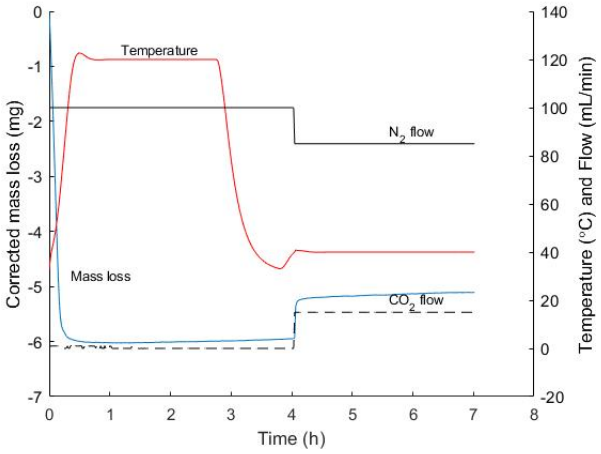

Figure 4.2: Result of a TGA measurement, showing temperature, N_2 and CO_2 flow and corrected mass loss of the sample over time.

$$q^* = \frac{\frac{m_{diff}}{MW_{CO_2}}}{m_{desorbed}} \qquad (4.1)$$

5 Results

The data on adsorption of CO_2 from direct air on Lewatit® VP OC 1065 in a fluidized bed was obtained using the setup described in chapter 4, using a single stage. To obtain the breakthrough curves, the sorbent circulation was shut down and the outlet concentration of CO_2 was measured over time, as the flow and concentration of the inlet were kept constant. These breakthrough curves were obtained for three different flow rates/superficial velocities, each with three different inlet concentrations (400, 600 and 800ppm), and each of these breakthrough measurements were done at two different bed heights (5 and 10 cm). The superficial velocities measured were 0.12 $m^3_{air}/(m^2_R.s)$, just above minimum fluidization, 0.17 $m^3_{air}/(m^2_R.s)$, when there is a visible bubble phase, and 0.23 $m^3_{air}/(m^2_R.s)$, with a significant bubble phase.

The output of these breakthrough measurements is the concentration of CO_2 in the outlet, in ppm. This is then converted into mol of CO_2 and divided by the mass of sorbent in the bed to obtain the loading of sorbent over time. The amount of sorbent in the bed, as it is a fluidized bed, depends on the superficial velocity of the gas phase. Based on the MSc thesis of R. Driessen and that of J. Linden [2, 32], the volume of the bed is composed of a solid phase, an emulsion phase, and a bubble phase. The emulsion phase is considered constant and equal to the emulsion phase at minimum fluidization (when the bubble phase is non-existent), having a constant void fraction of 0.51. The bubble phase, f_b, can be calculated by a correlation determined by J. Linden, which is a function of the excess superficial velocity, that is, $u_0 - u_{mf}$. At low excess superficial velocities, which is the case in the tested conditions, the correlation is linear and can be simplified to equation 5.2.

$$f_b = 1 - 1.014e^{-1.462(u_0 - u_{mf})} \tag{5.1}$$

$$f_b = 1.2775(u_0 - u_{mf}) - 0.0044 \tag{5.2}$$

The mass of sorbent in each set of conditions, this is, at each combination of bed height and superficial velocity, could then be determined. Its CO_2 loading over time was calculated through the measured outlet concentration over time and the amount of sorbent in the bed, as is represented in the Figures 5.1a and 5.1b, each obtained at a constant bed height of 5 an 10 cm, respectively.

It can be seen that, no matter the inlet concentration or bed height, the higher the flow rate, the faster the superficial velocity and the quicker the loading of the sorbent is. This is due to, for one, that a bigger quantity of CO_2 is provided to the system over time, therefore, there is more CO_2 available and coming into contact with the sorbent, which, considering the fast kinetics of the adsorption, will increase the driving force. Secondly, as the flow is more turbulent, there is better mixing of air and sorbent, and better mixing of loaded and lean sorbent within the bed. With a low flow rate and a superficial velocity close to minimum fluidization, the bed is loaded with CO_2 from the bottom to the top, similar to a fixed bed, and only the bottom layer comes into contact with fresh incoming gas. The top of the bed comes into contact with mostly lean gas, meaning, the driving force is very low at this place of the bed. As the superficial velocity increases, so does the bubble phase and with it the turbulence of the bed. This results in a better mixing of the sorbent, with a more homogeneous distribution of adsorbed CO_2 on the bed.

As for the final loading where the curve reaches the asymptotic value, it cannot be compared between experiments in their absolute value. Because the equilibrium loading of the sorbent is temperature dependent and the setup does not have temperature regulation on the adsorber, plus they were all performed on different

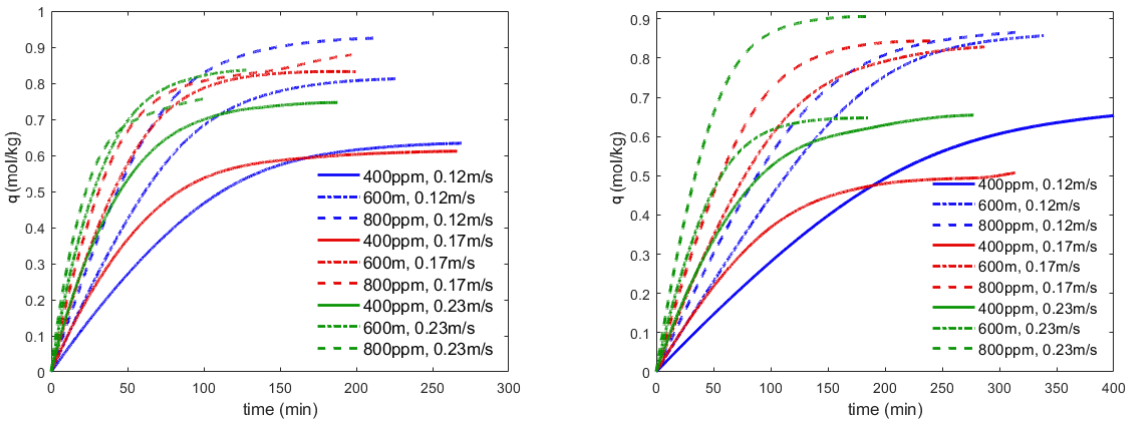

(a) Bed height: 5 cm

(b) Bed height: 10 cm

Figure 5.1: Sorbent loading (q) in mol_{CO_2}/kg in function of adsorption time for breakthrough curves obtained at 400(-), 600(-.) and 800(–) ppm inlet concentration and 0.12(blue), 0.17(red) and 0.23(green) $m^3_{air}/(m^2_R.s)$ of gas phase superficial velocity.

days, the temperature at witch the breakthrough curve was obtained differed from one experiment to the other. Therefore, the final loading of the sorbent can only be analyzed in its relative value, as the fraction of the theoretical equilibrium loading, obtained from the Toth isotherm described in chapter 2.

However, it was observed that when the loading reached a constant value, when the oulet concentration of CO_2 equaled the inlet concentration, this value was quite below the value obtained from the isotherm. Most breakthrough curves reached close to 70% of the isotherm equilibrium loading, which indicates that the sorbent within the setup had suffered some degradation. As the sorbent was not fresh when the experiments were started, and the same sorbent had been used in two assignments prior to this one, the degradation is to be expected. This indication was confirmed by TGA measurements of the sorbent, where the measured capacity of the sorbent was only 80% of the capacity determined by the isotherm. The TGA measurements are performed at 15% CO_2, which is quite higher than the 400-800 ppm (0.04-0.08%) at which the breakthrough curves where obtained, thus it is not clear if the degradation has the same consequences at a lower concentration of CO_2. In other words, it is not yet clear if a 20% loss of capacity at a certain set of conditions means a 20% loss of capacity at other conditions, or if the degree of degradation is dependent on the conditions of the measurement. Taking this uncertainty into account, and as the experimental results indicate to 70% of the isotherm value, this was the degree of degradation considered for the fraction of equilibrium loading achieved in the adsorption. The results of the TGA measurements, even though not applied directly, serve as confirmation of the sorbent degradation, and therefore justify the discrepancy of the experimental and theoretical equilibrium loadings. Therefore, this was taken into account when determining the relative loading of the sorbent over time, which can be seen in Figures 5.2a and 5.2b.

At a bed height of 5 cm, the lower the superficial velocity the higher fraction of equilibrium loading over stoichiometric time is achieved. This is an indication of the efficiency of the adsorption. The adsorption is more efficient under low flow rates, closer to minimum fluidization, as in this regime the bubble phase is very small, and therefore the contact of the solid and gas phase is bigger, with less mass transfer limitations. At a higher flow rate, even though the uptake is faster, as can be seen in Figure 5.1a, it is less efficient because of the bigger bubble phase and therefore bigger mass transfer limitations.

At a bed height of 10 cm, this variation of efficiencies with flow rates is less obvious, at least up to $t=t_{stoich}$. This is due to the height of the bed itself, as it increases the contact time between the gas phase and the solid phase and, in result, the effect of the bubble phase is less intense, even though it is still perceivable.

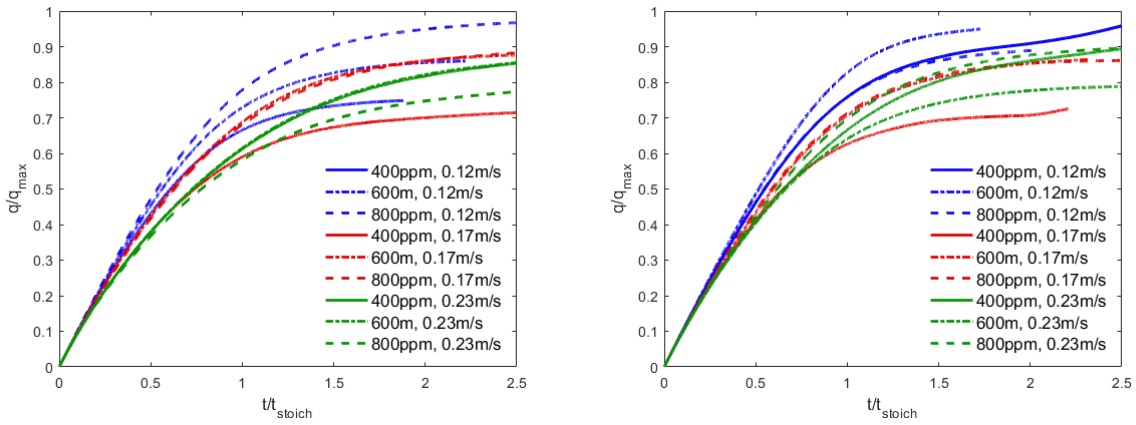

(a) Bed height: 5 cm

(b) Bed height: 10 cm

Figure 5.2: Relative loading of the sorbent in function of relative stoichiometric time for breakthrough curves obtained at 400(-), 600(-.) and 800(–) ppm inlet concentration and 0.12(blue), 0.17(red) and 0.23(green) $m^3_{air}/(m^2_R.s)$ of gas phase superficial velocity. q_{max} at 70% of the equilibrium capacity obtained from the Toth isotherm

For the purpose of this assignment, to design a setup that produces 1 kg/h of CO_2, it is more relevant that the sorbent adsorbs a large quantity of CO_2 in a short period of time, than that the adsorption is stoichiometrically efficient. So, from this assessment, a higher flow rate is more advantageous to achieve a higher CO_2 loading within the adsorption time. So at any given concentration of CO_2 in the inlet, superficial velocities of 0.17 to 0.23 $m^3_{air}/(m^2_R.s)$ provide a higher sorbent loading within a reasonable adsorption time.

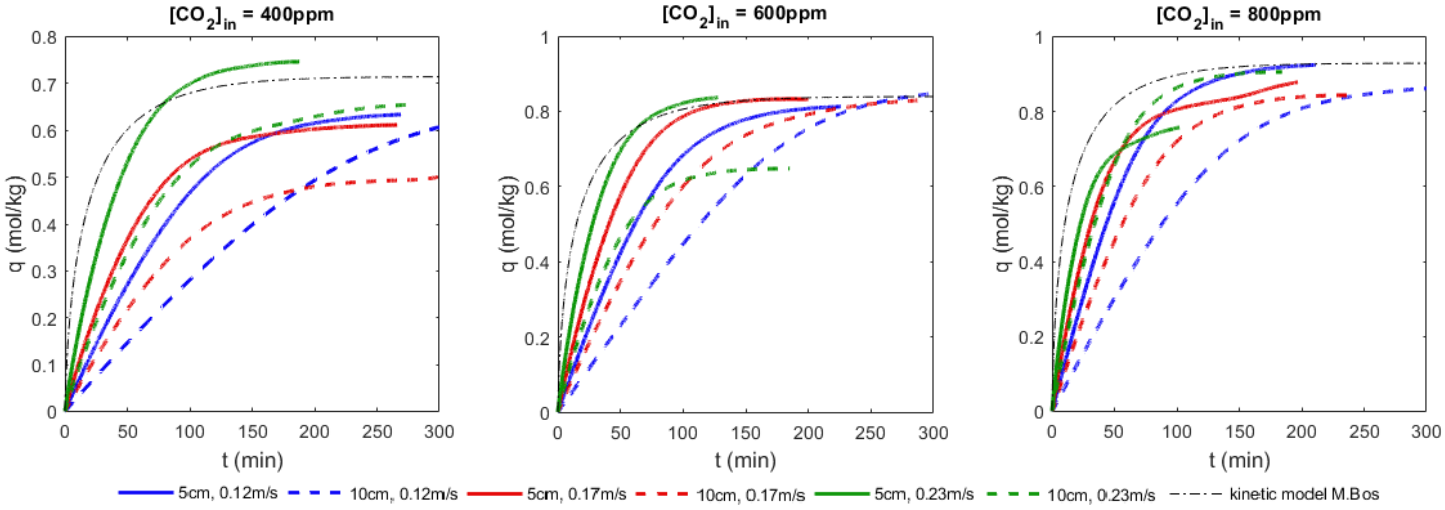

Figure 5.3: Sorbent loading (q) in mol/kg of CO_2 in function of adsorption time for breakthrough curves obtained at a bed height of 5 and 10 cm, and 0.12, 0.17 and 0.23 $m^3_{air}/(m^2_R.s)$ of gas phase superficial velocity. All three figures share the same legend.

When it comes to the bed height, the sorbent loading is faster at the more shallow bed. This is, of course, obvious as the taller bed contains twice as much sorbent, so theoretically the adsorption should take twice as long. In terms of fraction of equilibrium loading over the stoichiometric time, the curves for the two different bed heights should overlap, under ideal conditions. From Figures 5.4 it is visible that, even though the curves are close and overlap at first, they do not remain this way. This is because the conditions are not ideal and

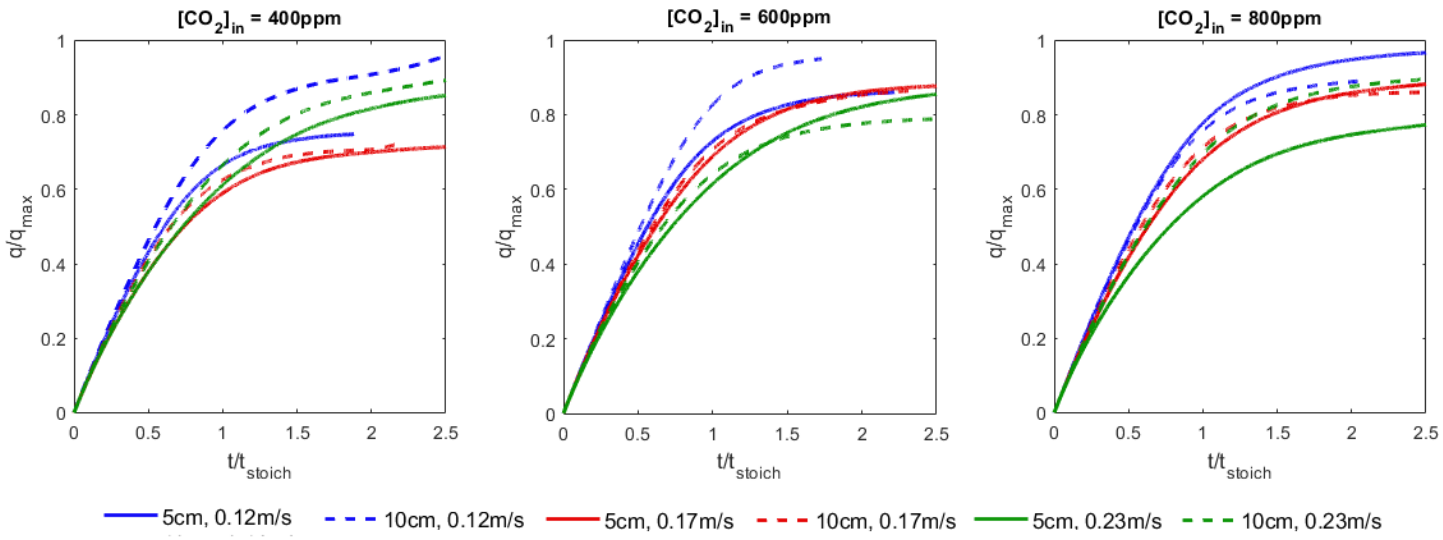

Figure 5.4: Relative loading of the sorbent in function of relative stoichiometric time for breakthrough curves obtained at 5 and 10 cm bed heights and 0.12, 0.17 and 0.23 $m^3_{air}/(m^2_R.s)$ of gas phase superficial velocity. All three figures share the same legend.

other factors play their part in the adsorption process, namely, once more, the mass transfer limitations due to the bubble phase. At 0.12 $m^3_{air}/(m^2_R.s)$, the taller bed is more efficient, at least at 400 and 600 ppm, because the contact time between the phases is longer, as has been mentioned before.

In Figures 5.3 the kinetic model obtained by M. Bos is also represented for comparison. This model is based on the Toth isotherm and the Toth rate equation, excluding any external mass transfer limitations. [33] Due to this exclusion, it is clear that the kinetic predicted by the model is faster than any of the experiments, where external mass transfer limitations cannot be neglected. Nonetheless, the breakthrough curves obtained at higher superficial velocities and in shallow beds are come within range of the ideal breakthrough curve predicted by the kinetic model.

Once more, it is important to keep in mind that the goal is to obtain a high sorbent loading in a short period of contact time, even if this does not coincide with the most efficient adsorption. From Figures 5.3 it is clear that, common to all three different inlet concentrations, both the 5 and 10 cm thick bed with 0.17 $m^3_{air}/(m^2_R.s)$ and 0.23 $m^3_{air}/(m^2_R.s)$ are the conditions at which this is achieved. For dimensional purposes for the reactor design, these are the operational conditions that will be considered.

6 Design Parameters

6.1 Sorbent flux

The amount of CO_2 obtained in the desorption, which is the ultimate goal in this setup design, is a function of the sorbent CO_2 loading, q, and of the sorbent flux. The higher the sorbent flux and the higher its loading the more CO_2 can be obtained in the desorption column. However, as the process is continuous and cyclic, the higher the sorbent flux in the adsorber, the lower is its residence time in the adsorber column, and therefore the lower its CO_2 loading is. This begs the question, is the production higher if the sorbent loading is high, but the sorbent flux low, or vice-versa?

The sorbent flux is inversely proportional to the residence time, for a fixed dimension of the adsorber. The sorbent loading over time can be determined from the breakthrough curves in chapter 5, which can be approximated to a 5th degree polynomial function for calculation purposes, even though the first period (up to approximately $0.5t_{stoich}$) is close to linear. This polynomial is a function of sorbent loading versus time. Even though the breakthrough curves were obtained for absolute time, in a circulating process it becomes sorbent loading versus residence time. This can be done because the sorbent flows from stage to stage, where it is always in contact with new air, that is, it mostly contacts with air in the same conditions as those for which the breakthrough curve was determined. While testing different values of residence time of the sorbent in the adsorber, both the resulting sorbent loading after leaving the adsorber and the sorbent flux can be calculated, maintaining the dimensions of the adsorber constant. With sorbent loading and sorbent flux, the amount of CO_2 obtained after desorption can be determined, in order to answer the pending question. The CO_2 obtained after desorption is calculated assuming the desorption is complete until equilibrium at desorption conditions. The detailed method of these calculations can be consulted in appendix A.5. Some values of residence time within a reasonable range (10 to 100 minutes) were represented in Figure 6.1, that were obtained from the breakthrough curve at 600 ppm and 0.23 $m^3_{air}/(m^2_R.s)$, to determine what the trend is.

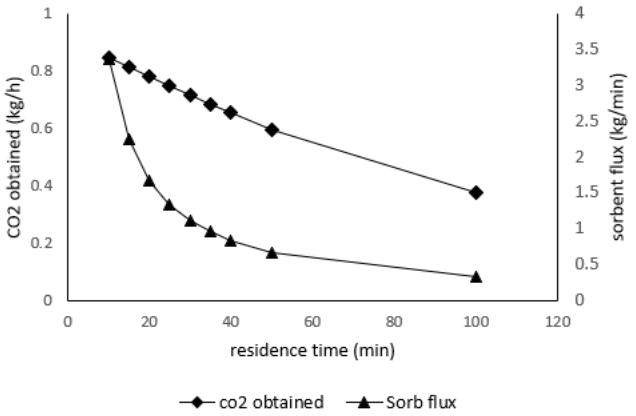

Figure 6.1: Effect of the residence time of the sorbent in the adsorber on the sorbent flux and amount of CO_2 obtained in the desorber, calculated with sorbent loading values from the breakthrough curve obtained at 600ppm and 0.23 $m^3_{air}/(m^2_R.s)$

It is clear that the amount of CO_2 obtained increases when the residence time decreases, even though the loading of the sorbent is lower. This is due to the fast increase of sorbent flux with the lower residence times. Furthermore, no matter how much the residence time increases, the higher sorbent loading will not

make up for the low sorbent flux, and the resulting production of CO_2 in the desorber will be lower the longer the residence time. With this, the conclusion is obvious that a lower residence time, thus higher sorbent flux, is advantageous. Nonetheless, high solid flows increase a lot the energy costs and the physical toll on the equipment, mainly the valves and riser. So a balance must be found, of high sorbent flux and low energy demands and maintenance costs. The main cost and energy demand associated to the circulation of sorbent is that of the riser, which transports the solids by an upward flow of air. So, the variation of the energy necessary to the riser with the variation of solid flux must be determined.

6.2 Riser

The energy required for the sorbent circulation can be narrowed down to the energy demand of the compression of the air flow in the riser, necessary to circulate the sorbent from the bottom of the desorber to the top of the adsorber. To determine the power necessary for compression, through equation 2.16, the necessary flow rate, superficial velocity of the air and pressure drop along the length of the riser need to be calculated.

The concept of the riser is of pneumatic transport, where solids are transported by a high enough flow of gas to overcome the gravity force. In pneumatic transport in vertical tubes, the solids should not represent more than 1% of the total flow, and the voidage of the flow should be between 0.999 and 0.980. Additionally, the solid to gas mass flow ratio should be lower than 10/20. Conventionally, pneumatic transport systems operate in a high gas velocity regime, of roughly $20u_t$ (where u_t is the terminal velocity of the particles) in order to prevent the settling or chocking of particles inside the tube. In very dilute systems, where the voidage is in the mentioned range, it is reasonable to assume there is no interaction between particles, and therefore the particle velocity is the same as the terminal velocity (u_p=u_t). [26]

The terminal velocity can be determined by the following correlation:

$$u_t = \Big[\frac{4d_p(\rho_s - \rho_g)g}{3\rho_g C_d}\Big]^{1/2} \tag{6.1}$$

where d_p is the particle diameter (668 nm [29]), ρ_s is the particle density (of the sorbent, 860 kg/m^3), ρ_g is the gas density (of air, at 20°C), g is the gravity force and C_d is the drag coefficient. The drag coefficient is determined by the following correlation, where Re_p is the Reynolds number for the particle, $Re = (\rho_p u_0 d_p)/\mu$, with μ the air viscosity at 20°C.

$$C_d = \frac{24}{Re_p} + 3.3643 Re_p^{0.3471} + \frac{0.4607 Re_p}{Re_p + 2682.5} \tag{6.2}$$

The mass flow of air to the compressor is determined assuming a 0.999 voidage, therefore, the air flow is proportional to the sorbent flux. The pressure drop along the length of the riser (about 3 meters) is calculated by adding the following factors:

$$p_2 - p_1 = \frac{\bar{\rho} g L sin\theta}{g_c} + \frac{u_s G_s}{g_c} + \Delta p_f \tag{6.3}$$

The three terms account for the static head, the kinetic energy of the solids, and the frictional resistance of the mixture with the pipe wall. This last term, $Deltap_f$, is determined by the following equation,

$$\Delta p_f = \Delta p_{f,g} + \Delta p_{f,s} = \frac{2 f_g \rho_g u_g^2 L}{g_c d_t} + \frac{2 f_s G_s u_s L}{g_c d_t} \tag{6.4}$$

Where u_g is the gas velocity and u_s is the velocity of the solids and G_s is the solid mass flow. The gas friction

factor, f_g, is a function of the tube's Reynolds number and, for $10^5 < Re_t < 10^8$, it's determined by

$$f_g = 0.0008 + 0.0552 Re_t^{-0.237} \tag{6.5}$$

For f_s, the solid friction factor, near atmospheric conditions, the following equation can be used,

$$f_s = \frac{0.05}{u_s} \tag{6.6}$$

$\bar{\rho}$, the average density of the mixture, can be determined simply by

$$\bar{\rho} = \rho_s(1 - \varepsilon_g) + \rho_g \varepsilon_g \tag{6.7}$$

With the previous equations and correlations [26], the adiabatic compression power necessary for the riser to transport a certain solid flow can be calculated. The relation between the sorbent flux and the compression power, as well as the amount of CO_2 obtained in the desorption in function of the sorbent flux (obtained from Figure 6.1) can be analyzed in Figures 6.2a and 6.2b.

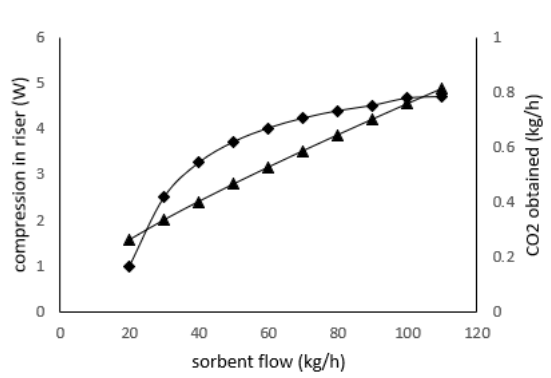

(a) Maintaining u_g=20u_t

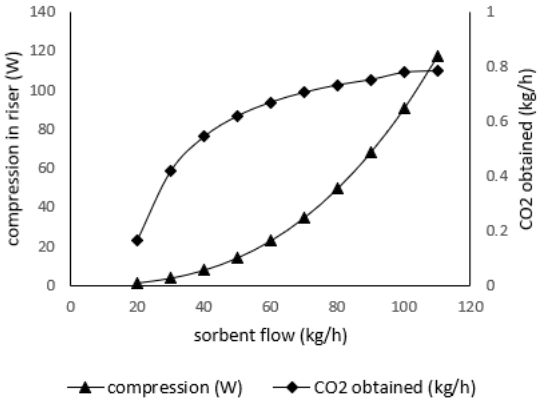

(b) Maintaining the pipe diameter = 8 cm

Figure 6.2: Relation between the adiabatic compression of the riser air flow and the sorbent flow, and of the CO_2 obtained in the desorption with the sorbent flow (for a study case of using 600ppm air under 0.23 m/s in 10 adsorption stages)

It is clear that, from a certain sorbent flux (around 60 kg/h) there is no significant increase in the amount of CO_2 obtained. This is when the increase in sorbent flux and the decrease of sorbent loading are close to canceling each other out. Meanwhile, the necessary compression power steadily increases with the increase of the solid flow, even in the case of Figure 6.2a where the diameter of the riser increased with the sorbent and air flow, and the gas superficial velocity was maintained relatively constant. So, it is a reasonable choice to use a sorbent circulation rate of 60 kg/h as it maximizes the amount of CO_2 produced in the desorber, at a relative low cost to the air compression in the riser. On Figure 6.2b, the fast increase of compression power occurs just above 60 kg/h, which justifies this choice.

For 60 kg/h, and for a voidage of 0.999 in the riser, the necessary flow rate of air is 70 m^3/h, in a riser with 8 cm of inner diameter and a air superficial velocity of 3.8 m/s.

6.3 Adsorption column dimensions

With a defined sorbent flow, the residence time of the sorbent in the adsorber can be defined as well, although it still depends on the number of stages and the height of each stage. A maximum number of stages was set at 10, seeing as this corresponds to an adsorber column of about 2 meters (each stage with 20 cm), and the maximum thickness of the beds at 10 cm. A thicker bed would increase the bubble phase and decrease the contact efficiency of the bed. Considering that greenhouses have a height of between 3 and 10 meters high, it is not wise to design a reactor that does not fit in the smaller greenhouses. With 10 stages and 60 kg/h of sorbent, the four most favourable operating conditions were compared in terms of CO_2 production in the desorber. They can be graphically compared in the following figure.

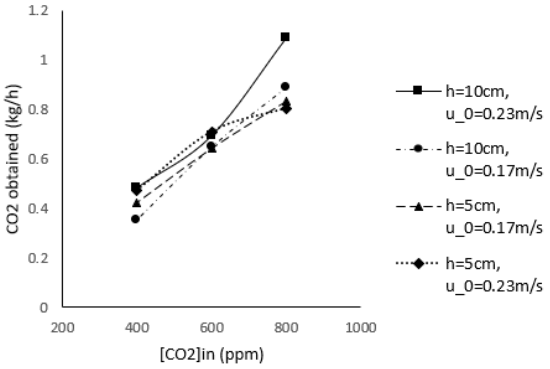

Figure 6.3: CO_2 production capacity of the desorber in different conditions of bed height and superficial velocities of the inlet air, for 10 stages and sorbent circulation at 60 kg/h in the 400-800ppm range of CO_2 concentration in the inlet air to the adsorber.

For the tested conditions, between 400 and 600 ppm in the treated air in the adsorber, the production of CO_2 in the desorption is quite similar for all. This, however, changes at the higher inlet concentration of 800 ppm, at 10 cm tall beds and 0.23 m/s of superficial velocity, as the production is quite higher than at the other three conditions. Besides, these conditions are the only ones that are capable of providing the goal of 1 kg/h of CO_2, even if this is only possible when the inlet concentration is 800 ppm. For the other operation modes to be able to produce this quantity of CO_2, or for this to happen no matter the inlet concentration, more stages would be necessary. The design goal requires, therefore, some adjustments. As it is, an adsorber with 10 stages, each stage with 10 cm bed height, operating at a superficial velocity of 0.23 m/s and a sorbent flow rate of 60 kg/h, has a sorbent residence time of 34 minutes. The sorbent loading exiting the adsorber is determined based on 2 assumptions: the first one is that the sorbent entering the adsorber already has a loading of 0.21 mol/kg, the equilibrium loading at 400 ppm and 70°C (desorption conditions); the second assumption is that the sorbent loading after a certain residence time in the adsorber is equivalent to the loading after that same time in a closed system - the loading at residence time (RT) is the same as the loading at t=RT from the breakthrough curve.

This second assumption is made because, at each stage, the sorbent contacts new air, and not air that comes from the stage below. This way, the sorbent flow in the adsorber can be compared to 10 CSTRs in series, with air in cross-flow. This assumption can unfortunately not be validated experimentally, as the MSFB setup only has one air inlet at the bottom and one air outlet at the top, and the air flows through all consecutive stages (comparable to a Plug Flow Reactor).

6.4 Desorption column dimensions

Based on these assumptions, the sorbent will leave the adsorber with a CO_2 loading between 0.39 to 0.62 mol/kg, depending on the air inlet concentration. The desorber works as a Plug Flow Reacto in counter-current, with sorbent flowing from stage to stage through the downcomers, and the air flowing up through all stages, at 70°C. The stages are heated by flowing hot water around the walls of the desorber and by heating the plates where the beds rest upon. As the fluidization mixes the sorbent within the bed and promotes heat transfer by forced convection, it can be assumed that the temperature is homogeneously distributed through the bed. However, on the top stage of the desorber, cold sorbent falls into the bed, so it is important to determine if this has a relevant effect on the overall temperature of the stage. As the air flowing trough the top stage has passed the bottom ones already, it is safe to assume the air is at 70°C, and this will heat the sorbent particles, after being immersed in the bed, by forced convection and conduction. To evaluate if there are heat transfer limitations, the internal and external heat transfer rate on the sorbent particles should be determined. The external heat transfer coefficient can be determined with the dimensionless Nusselt number by the following correlation with the particle's Reynolds and Prandtl number [34].

$$Nu = 2 + 0.6Re^{1/2}Pr^{1/3} \tag{6.8}$$

with $Pr = (C_p\mu)/\lambda_{air}$, where μ is the viscosity of air at 70°C, 2.05×10^{-5} kg/(m.s) [35], C_p is the heat capacity of the sorbent, 1.58 KJ/(kg.K) [33] and λ_{air} is the thermal conductivity of the air at 70°C, 29.5 mW/(m.K) [35]. The heat transfer coefficient, h, can then be calculated with the formula:

$$Nu = \frac{hd_p}{\lambda_{air}} \tag{6.9}$$

The resulting heat transfer coefficient is 1.8×10^3 W/(m^2.K).

As for the internal heat transfer, to determine if the conduction inside the particle is faster than the the convection on its surface, the Biot number can be used. The Biot number is used as an indication to determine where the major resistance to heat transfer lies, in the interior of the particle or on the surface. [36]

$$Bi = \frac{hL_c}{\lambda_s} \tag{6.10}$$

L_C is here the characteristic length which is commonly defined as the volume of the particle divided by the surface area of the particle [37] and λ_s is the conductivity of the sorbent. The characteristic length is determined using the average diameter of the particle of 688 mm, surface area of 50 m^2/g and density of 880 kg/m^3. [14] If the Biot number is smaller than 1, the resistance to heat transfer lies on the interface between the particle and the surroundings. If the Biot number is much smaller than 1, the temperature inside the particle can be considered uniformly distributed, thus the resistance lies solely on the surface.

Using the conductivity of the sorbent, λ_s, of 0.43 W/m.K [33] and heat transfer coefficient, $h = 1.8\times10^3$ W/m^2.K, obtained from equation 6.8, the Biot number is 9.6×10^{-5}, which is much smaller than 1. Therefore, it is reasonable to assume that the temperature inside the sorbent particle is uniform, and that the resistance to heat transfer is on the surface, therefore, the heat transfer limitations are external.

Knowing the heat transfer coefficient, and that the resistance lies on the surface, the time it takes for the sorbent to reach the desorption temperature once immersed in the desorption bed can be determined. This can be determined the following way:

$$hA(T_\infty - T)dt = mC_pdT \tag{6.11}$$

With $m = \rho V$ and $dT = d(T - T_\infty)$ the previous equation becomes

$$\frac{d(T - T_\infty)}{T - T_\infty} = -\frac{hA}{\rho V C_p} dt \tag{6.12}$$

Which can be then integrated from t=0 to t and T=T_i to T(t) and

$$\frac{T(t) - T_\infty}{T_i - T_\infty} = e^{-bt} \tag{6.13}$$

$$b = \frac{hA}{\rho V C_p} \tag{6.14}$$

The higher the value of b, the faster the temperature of the particle reaches the temperature of the surroundings. For the sorbent particle, the value of b is 5.7×10^4 which means that the particles reach 70°C very quickly, and therefore, heat transfer is not an issue.

What remains to be verified, is if the residence time of the sorbent in the desorber is sufficient for full desorption until equilibrium at 70°C and air as purge gas. Qian Yu, *et. al*, [15] studied the desorption of sorbent after direct air capture in one tall fluidized bed using air as purge, at temperatures between 67 and 72 °C, at different residence times. They concluded that the desorption is more kinetic than equilibrium controlled. An increase in residence time, from 10, to 18 and 34 minutes, increased both the working capacity of the sorbent and average CO_2 concentration in the product gas, in a continuous operation. High air flow rates are also required for high sorbent working capacity. The 55 m^3/h required for 1 kg/h of CO_2 in the form of 1% CO_2 enriched air may not be enough to desorb the sorbent to equilibrium within the short residence time of 23 minutes (residence time for 5 stages of 10 cm each). Thus, it may be necessary to increase the air flow, even though, with it, the concentration of CO_2 in the product stream decreases. Considering the heat transfer was found to be a dominating parameter in the desorber [15], a high flow rate of purge air is is not only advantageous in increasing the driving force of the desorption reaction, but also in increasing the heat transfer efficiency.

The studies done on desorption of CO_2 from Lewatit® VP OC 1065 all start from fully or almost fully adsorbed sorbent, at close to equilibrium capacity [31, 38, 15, 3]. In those experiments, the initial desorption is fast, and once equilibrium is approached it slows down. In many experiments, the residual loading at the end is around 0.5 mol/kg. The results of desorption with nitrogen as purge, at atmospheric pressure, and different temperatures, obtained by Vincent Kroeze [3] are shown in Figure 6.4

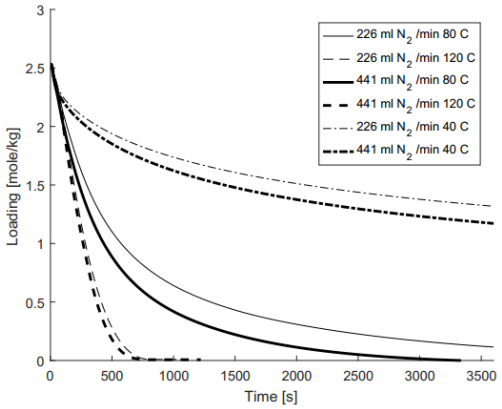

Figure 6.4: Desorption curves using a 226 and 441 ml/min N_2 purge at 80 and 120°C and 1 atm in a fixed bed. [3]

This data seems to indicate that the desorption from low loadings of CO_2 to even lower ones (as, in the intended case, from ∼0.5 mol/kg to 0.21 mol/kg) takes a very long time, at least a few hours. However, these studies where done in a fixed bed, and the study of Qian Yu, *et. al.*, [15] previously described, is performed in one very tall fluidized bed (6 cm diameter by 2 m length). Fluidized beds have proven to be more efficient, as has been previously explained, and multi-stage fluidized beds have been demonstrated to be quite more efficient than single stage, as it reduces heat transfer limitations, reduces bypassing and increases contact of the two phases. In one tall fluidized bed, because the bubbles increase in size from the moment they are formed to the moment they are release from the bed, the contact efficiency between gas and solid phase is lower than in multiple shallow beds, where the bubbles have less time to develop into large bubbles. All of this information indicates that, in a multi-stage fluidized bed, with proper heat transfer, the desorption, even at low CO_2 loadings, is more efficient than in the previously studied contactors.

It was not possible to test these specific conditions in the same setup used for the breakthrough curves, described in chapter 4 but, despite this, it was possible to perform the desorption at 70°C with nitrogen as purge with low initial CO_2 loading of the sorbent and short sorbent residence times. Two different residence times were tested, 12 and 18 minutes, under the same adsorption conditions (0.14 m/s at 2065ppm inlet concentration, the maximum possible, at room temperature) and the same desorption conditions (0.14 m/s of pure N_2 at 70°C). The outlet concentrations of the adsorber and the desorber at stationary state, as well as the desorption and adsorption capacity of the sorbent can be seen in the following Figure 6.5. Even though the loading of the sorbent after adsorption (q_{ads}) is far below the loadings that would be interesting to study, it can be seen that the desorption capacity is very close to the adsorption value. This means that most of the adsorbed CO_2 is desorbed within the residence time of the desorber. Thus, despite the low values, the desorption is still relatively fast in these conditions of multi-stage fluidized bed at 70°C.

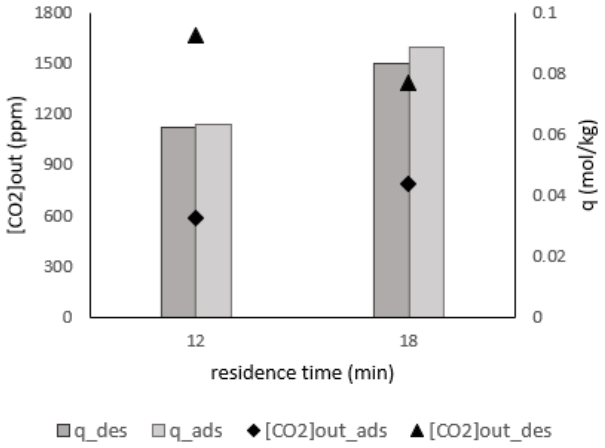

Figure 6.5: Effect of residence time on the adsorption and desorption capacity (q_{ads} and q_{des}) and average CO_2 concentration in the adsorber and desorber outlet.

Even though this experimental data is by no means conclusive about the specific results of the desorption in the designed setup, it gives an indication about the desorption at low initial loading of CO_2 on the sorbent. Despite the reduced driving force in absolute numbers, the effective heat transfer, the good mixing within the stages and the high gas to solid ratio increase the rate of desorption. Therefore, the desorption can still be effective within a small time frame, under these conditions.

The assumption that in 23 minutes of residence time, at 70°C with air as purge at a flow rate of 55 m^3/h, the sorbent loading is reduced from between 0.39 and 0.62 mol/kg to 0.21 mol/kg cannot be validated at this point. However, the results of Qian Yu, *et. al.*, support this assumption, as it produced a continuous product gas with 1% CO_2 with a sorbent residence time of 34 minutes and a similar superficial velocity.

7 Final Design

7.1 Adsorption column

As has been mentioned in chapters 5 and 6, at a higher flow rate and superficial velocity of air, the uptake of CO_2 on the sorbent is faster. However, as the loading increases, the efficiency of the adsorption under high superficial velocities decreases compared to that of lower superficial velocities. So, as it is advantageous to have a high flow rate of air when the sorbent has a low loading, and smaller flow rate when it increases, a simple solution presents itself. Instead of the flow rate of incoming air being equally distributed through the 10 stages of the adsorber, it can be unequally distributed, with the higher flow rate to the top stages and a lower one to the bottom stages. On the top stages, the sorbent loading is so low that the uptake rate is mostly limited by the amount of CO_2 provided, so if more CO_2 is provided, resulting of a higher flow rate, more CO_2 is is adsorbed. As the sorbent loading increases and the driving force decreases, the uptake rate is less dependent on the amount provided and more dependent on the contact efficiency of the two phases. This means, that a superficial velocity closer to minimum fluidization is more advantageous, because the bubble phase is reduced.

So, in this sense, the flow rate was distributed through the 10 stages as shown in Table 7.1, with high superficial velocities in the top 4 stages, a medium one in the following 4, and close to minimum fluidization on the last 2, where the more efficient contact between phases is more relevant given the higher loading of the sorbent.

Table 7.1: Description of the stages in the adsorber, with superficial velocity, corresponding flow rate, residence time and pressure drop across the bed. Stages are numbered from top to bottom.

stages	$\mathbf{u_0}$ **($\mathbf{m^3_{air}/m^2_R.s}$)**	**flow rate ($\mathbf{m^3/h}$)**	**residence time (min)**	**pressure drop (Pa)**
1-4	0.305	138	2.4	185.2
5-8	0.220	99.5	3.5	276.7
9-10	0.120	54.3	4.9	384.3
TOTAL	-	1059	33.5	2616

7.2 Desorption column

The design for the desorber is a 5-stage fluidized bed with 40 cm diameter, operating at 70°C and 0.14 m/s of air superficial velocity. The total residence time of the sorbent, which circulates at a flux of 60 kg/h, is 23 minutes. However, despite what has been described in chapter 6, it is not advantageous to have all stages with the same height and thus, with equal sorbent residence time. This is mainly because, on the top stage, the purge air already has a significant concentration of CO_2 and, as the loading of the sorbent is not so high to start with, the loading on the sorbent is close to the equilibrium loading at that set of temperature and CO_2 concentration. On this stage, there may even occur adsorption, to some degree. However, as the loading of the sorbent is close to the equilibrium loading at said conditions, the adsorption rate is so low that it will not be significant given a short contact time of solid and gas phases. At the same time, the driving force for desorption is low and no significant CO_2 is released from the sorbent to the air on this stage. Given these

aspects, the residence time in the top stage should be short, and this stage's purpose is that of increasing the temperature of the sorbent to desorption temperature. To reduce the residence time, without changing the sorbent flux, the bed height must be decreased which, in turn, increases the heat transfer efficiency because it decreases the volume to heat transfer area ratio. With a bed height of 3 cm, the residence time is about 1.4 minutes, which theoretically is enough time for the sorbent's temperature to increase to 70°C.

For similar reasons, the second stage from the top should also have a shorter residence time then the one below, which should have a shorter residence time than the next one, and so forth. This way, the bed height increases from top stage to bottom stage. Because the sorbent and air contact in cross-flow, on the bottom stage the air is leanest and the sorbent is heated at 70°C, therefore heat transfer is not a limitation on this stage and the bed can be tall, at 15 cm. This allows more contact time of the sorbent with the air and, because the bubble phase is not a big issue at a superficial velocity of 0.14 m/s, a more efficient desorption until equilibrium. On this stage, the sorbent is, however, already close to being lean so, on the second to bottom stage the air does not have a very high concentration of CO_2, therefore can still desorb efficiently. Thus, this stage can also have a high residence time, meaning, a taller bed of 15 cm. On the third and middle stage the CO_2 concentration is already higher, so a more shallow bed, of 10 cm, is more reasonable, to decrease the contact time and allow the desorption reaction to favour above the adsorption one. On the second to top stage, this is even more pressing, therefore, the contact time should be even shorter, decreasing the bed height to 7 cm. This way, the total residence time of the sorbent in the desorber remains the same, 23 minutes, but it is unevenly distributed through the stages, increasing from top to bottom.

It is important to note that, even though the concentration of CO_2 in the air stream can be estimated in relative terms, the precise concentration or the variation of the desorption efficiency with contact time are not known, because the desorption in these conditions could not be studied with the available setup.

The table below, 7.2, shows the bed thickness, residence times and pressure drop (calculated with equation 2.9) of each stage, as well as the total.

Table 7.2: Description of the 5 stages in the desorber, with bed thickness (when fluidized), corresponding residence time and pressure drop across the bed. Stages are numbered from top to bottom.

stage	**bed thickness (cm)**	**residence time (min)**	**pressure drop (Pa)**
1	3	1.4	108.2
2	7	3.2	252.6
3	10	4.6	360.8
4	15	6.9	541.2
5	15	6.9	541.2
TOTAL	50	23.1	1804.1

The final design for the setup can be seen in figures 7.1 and 7.2.

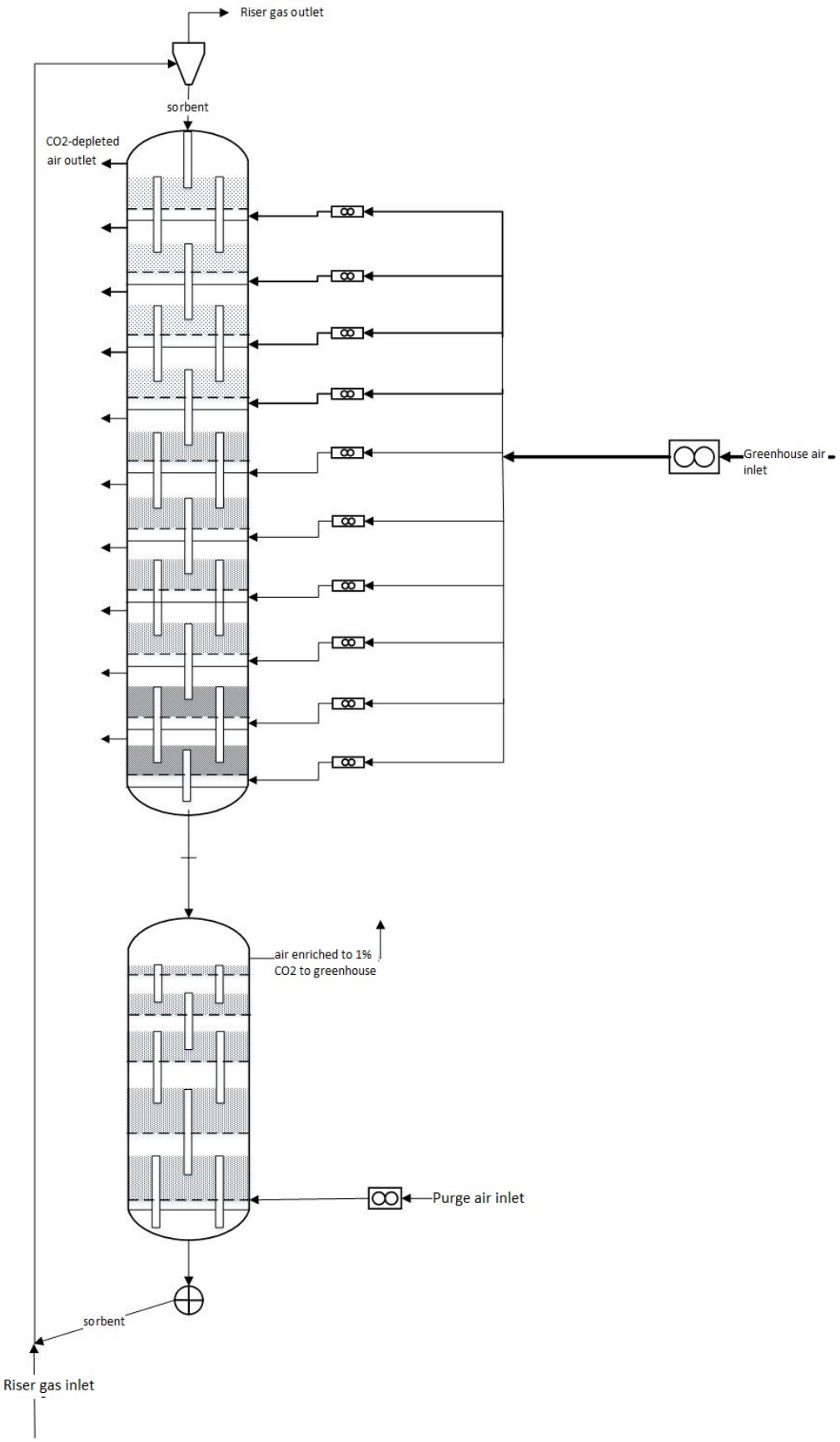

Figure 7.1: Inside view of the final design of the setup.

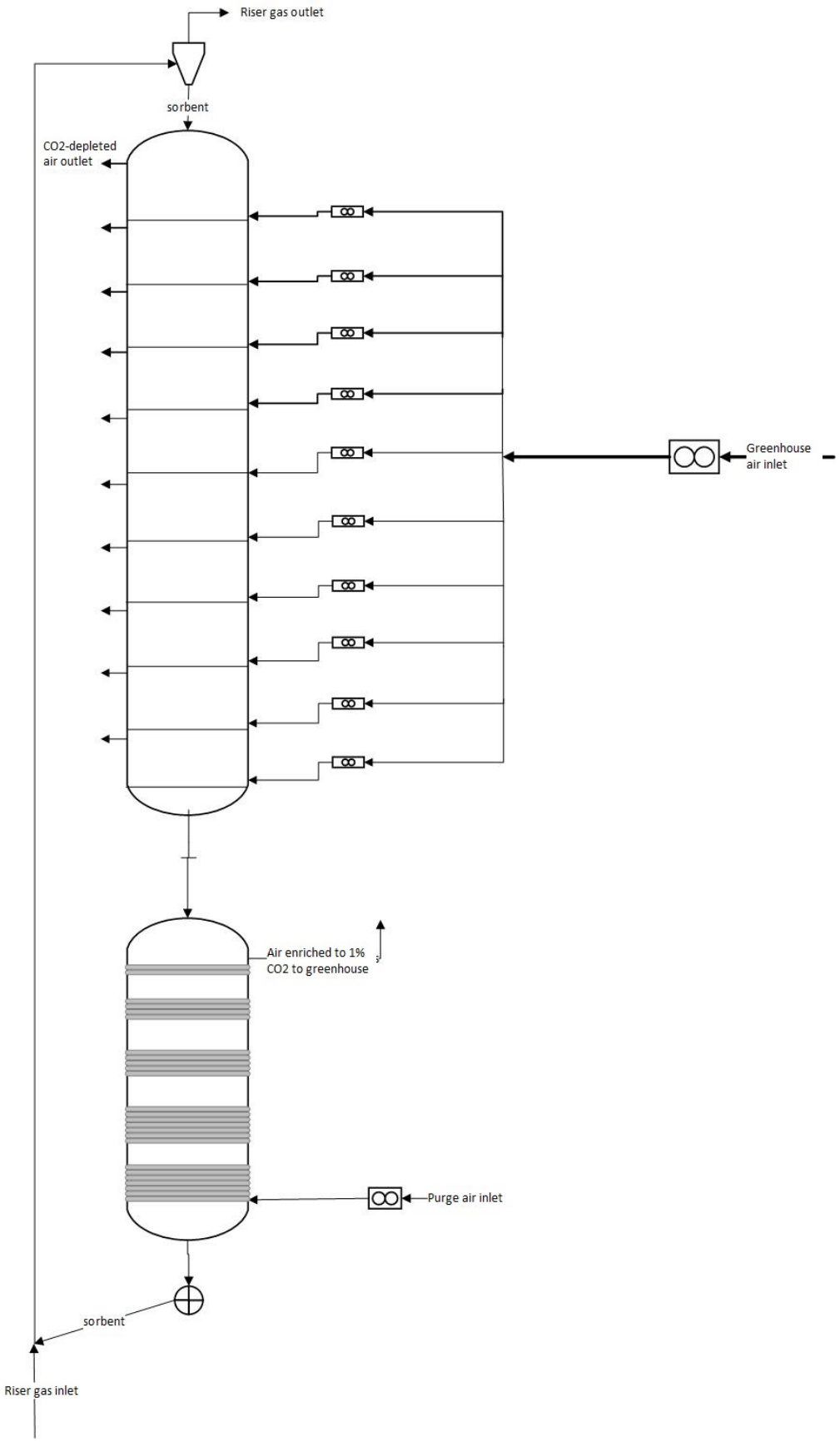

Figure 7.2: Outside view of the final design of the setup. Heat tracing around the desorber stages.

7.3 Energy cost analysis

In order to estimate the overall energy demands of operating the setup, the calculations described in chapter 2 by equations 2.12 to 2.16 can be used once more, now applied to the final design described above. It is important to note that the energy demands are obtained in units of kJ per kg of desorbed CO_2 which, given the efficiency of the desorption process, corresponds to 1.7 kg CO_2 actually on the sorbent, which is relevant for the calculation of the heat to be provided in the desorber to increase the temperature to 70°C. Another important note is that, despite the goal of producing 1 kg/h of CO_2, the average and pessimistic value of 1 kg of CO_2 per 1.3 hours was used.

The energy demand values of the different factors in the operation of this setup are seen in Table 7.3 and in relative terms in Figure 7.3. From the figure it is clear that the biggest energy penalty is, by far, the energy spent on compressing the air that goes into the adsorber, making up almost three quarters of the total energy requirements. This is due to the fact that every one of the 10 stages has a separate inlet flow of air, unlike the desorber. In the desorber, not only is the total flow rate of air a lot smaller than in the adsorber, but the pressure drop along all stages is cumulative. This is not the case in the adsorber, where in every stage the weight of the bed has to be overcome by a different stream, and a different fan.

$Q_{reactheat}$	1.5×10^3
$Q_{senssorb}$	6.2×10^3
$Q_{compads}$	2.2×10^4
$Q_{compdes}$	1.3×10^2
$Q_{compriser}$	1.2×10^1
Q_{sensco_2}	7.2×10^1
Total	3.0×10^4

Table 7.3: Energy costs of the different operations of the setup in kJ/kg of desorbed CO_2.

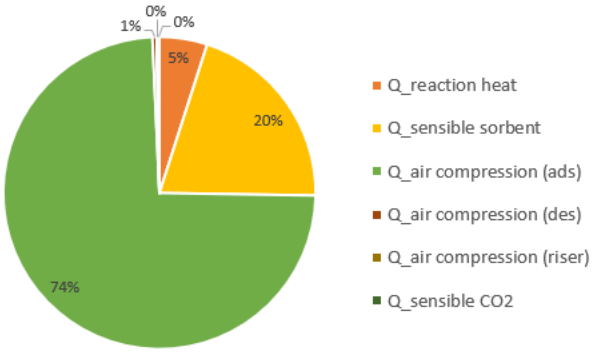

Figure 7.3: Relative energy costs of the different operations of the setup.

By comparison, the contribution of the compression energy of air for the desorber and riser, and the energy necessary for the heating of the CO_2 are negligible. Therefore, in terms of economic analysis of operating this setup, the most relevant parameters are the contacting energy demand and costs in the adsorber, in terms of electric costs, and the heating in the desorber, in terms of thermal energy.

The contacting energy, as described by Qian Yu [39], is calculated by the following equation A.2, where η_g is the gas efficiency of adsorption, determined by equation A.3.

$$E(J/g) = \frac{\Delta P(Pa)}{\eta_g . C_{CO_2}(g/m^3_{air})} \tag{7.1}$$

$$\eta_g = \frac{C_{CO_2}.t - \int_0^t C_{CO_2} dt}{C_{CO_2}.t} \tag{7.2}$$

Because in each adsorption stage new air is contacted with the sorbent, the gas efficiency has to be calculated for each stage and not as a whole unit. For calculation purposes, the average inlet concentration of 600 ppm was used, as well as the breakthrough curve at this concentration, obtained from chapter 5, to determine the integral. The detailed calculations can be consulted in the appendix A.6.

The sum of the contacting energy of all adsorption stages is approximately 3.5 kJ/g_{CO_2}. With the cost of

electricity, C_{elect}, the contacting cost, C_{cont}, can be determined, using the conversion described in equation 7.3 [39]. The cost of electricity for businesses in the Netherlands, is estimated at 0.16 €/kWh [40].

$$C_{cont}\left(€/kg_{CO_2}\right) = \frac{E(J/g)}{3.6 \times 10^6 (J/kWh)}.C_{elect}\left(€/kWh\right) \times 10^3 (g/kg) \tag{7.3}$$

Given this, the contacting cost of the adsorption process is 0.15 €/kg_{CO_2}.

As for the cost of regeneration of the sorbent, C_{reg}, these are mostly composed of the cost of the thermal energy required to heat up the sorbent and to overcome the endothermicity of the desorption reaction. Qian Yu [39] simplified this calculation as described in equation 7.4.

$$C_{reg}\left(€/kg_{CO_2}\right) = \left(\Delta H_r(kJ/g) + \frac{C_{p,sorb}(kJ/kg.K).(T_{des} - T_{ads})(K)}{(q_e - q_{des})(mol/kg).\eta_s.MW_{CO_2}(g/mol)}\right).C_{therm}(€/GJ) \tag{7.4}$$

$$\eta_s = \frac{q_t - q_{des}}{q^* - q_{des}} \tag{7.5}$$

ΔH_r is the heat of reaction, 65 kJ/mol [31], η_s is the solid efficiency, calculated with equation 7.5, where q_t is the sorbent loading at the end of the adsorption process, here using the average value of 0.47 mol/kg, and the thermal energy cost, C_{therm}, from natural gas for businesses in the Netherlands is estimated at 3.44 €/GJ [41]. The final cost of the desorption is, thus, 0.03 €/kg_{CO_2}.

Considering that the goal of producing 1 kg of CO_2 an hour is achieved, with higher concentrations of CO_2 in the air and non-degraded sorbent, the cost of operating the setup is set at 0.18 €/h, or 180 €/ton_{CO_2}. If it is working continuously for 14 h/day, during sunlight hours, the daily operation cost is merely 2.5 €/day, measuring to 76 €/month.

The cost of industrial CO_2 is between 80 and 180 €/ton. This means that running the air capture setup has the same cost than the more expensive supply of industrial CO_2. However, in a future where CO_2 emissions get taxed, it may end up being cheaper to use this installation in industrial greenhouses. Besides, just like many of the sustainable measures, the cost barrier does not justify lack of initiatives to reduce emissions of pollutants, given their environmental impact.

7.4 Conclusion and Recommendations

Regarding the final design and the process followed to reach it, a few important notes need to be discussed. It's important for the reader to retain that this is a preliminary design, obtained from preliminary data and calculations.

Firstly, the breakthrough curves, on which the values of sorbent loading and amount of CO_2 adsorbed were based on, were obtained with somewhat degraded sorbent. This was confirmed with the TGA measurements. This indicates that, using fresh non-degraded sorbent in the installation, the sorbent loading leaving the adsorber is higher than the one determined and, therefore, more CO_2 can be desorbed and a higher concentration on the product stream can be achieved. However, even though the equilibrium loading under these conditions with fresh sorbent can be estimated using the Toth isotherm and its parameters, determined by M. Bos [1], the uptake rate and shape of the resulting breakthrough curve cannot be accurately predicted. This way, the calculations of sorbent loadings and production of CO_2 enriched stream in the designed setup should be seen as those of a pessimistic scenario, when the sorbent approaches the end of its lifetime, with the confidence that it is more efficient through most of the operation of this installation.

Given this, the calculated costs are higher than the resulting costs of using non-degraded sorbent. This

because the operation costs remain the same, but the amount of CO_2 obtained is higher. These costs are determined based only on operation, excluding investment costs and maintenance. For a fully detailed economic analysis, more extensive data and calculations would need to be performed, mainly data on adsorption in this setting of cross-flow, validating the approximation of using residence time in a stage as absolute time in the closed stage where the breakthrough curve was obtained, and more extensive data on the desorption under the selected conditions.

Furthermore, the data obtained and the calculations made were for dry air, neglecting the humidity in the air in the greenhouse. This is a very important factor, because it is known that the presence of water increases the CO_2 capture capacity of the sorbent, but also increases the heating requirements of the desorption process. Therefore, for further development of this setup, also this aspect requires further study.

Bibliography

[1] M. Bos, *Storage of renewable electricity in methanol: Technology development for CO_2 air capture and conversion to methanol*. PhD thesis, 06 2019.

[2] R. T. Driessen, "Development of a multistage fluidized bed for deep h_2s removal from natural gas," Master's thesis, University of Twente, 2016.

[3] V. Kroeze, "Co_2 capture with supported amine sorbent - evaluation of desorption conditions," Master's thesis, University of Twente, 2016.

[4] R. A Khatri, S. Chuang, Y. Soong, and M. Gray, "Thermal and chemical stability of regenerable solid amine sorbent for co_2 capture," *Energy & Fuels - ENERG FUEL*, vol. 20, 07 2006.

[5] K. S. Lackner, S. Brennan, J. M. Matter, A.-H. A. Park, A. Wright, and B. van der Zwaan, "The urgency of the development of co_2 capture from ambient air," *Proceedings of the National Academy of Sciences*, vol. 109, no. 33, pp. 13156–13162, 2012.

[6] A. A. Olajire, "Co_2 capture and separation technologies for end-of-pipe applications – a review," *Energy*, vol. 35, no. 6, pp. 2610 – 2628, 2010. 7th International Conference on Sustainable Energy Technologies.

[7] B. Dutcher, M. Fan, and A. G. Russell, "Amine-based co_2 capture technology development from the beginning of 2013—a review," *ACS Applied Materials & Interfaces*, vol. 7, no. 4, pp. 2137–2148, 2015. PMID: 25607244.

[8] R. S. Haszeldine, "Carbon capture and storage: How green can black be?," *Science*, vol. 325, no. 5948, pp. 1647–1652, 2009.

[9] M. Sánchez-Guerrero, P. Lorenzo, E. Medrano, N. Castilla, M. Soriano, and A. Baille, "Effect of variable co_2 enrichment on greenhouse production in mild winter climates," *Agricultural and Forest Meteorology*, vol. 132, pp. 244–252, 10 2005.

[10] S. Kim, H. Shi, and J. Y. Lee, "Co_2 absorption mechanism in amine solvents and enhancement of co_2 capture capability in blended amine solvent," *International Journal of Greenhouse Gas Control*, vol. 45, pp. 181 – 188, 2016.

[11] E. Erdal Ünveren, B. Özmen Monkul, S. Sarıoğlan, N. Karademir, and E. Alper, "Solid amine sorbents for co_2 capture by chemical adsorption: A review," *Petroleum*, vol. 3, 12 2016.

[12] R. Veneman, N. Frigka, W. Zhao, Z. Li, S. Kersten, and W. Brilman, "Adsorption of h2o and co_2 on supported amine sorbents," *International Journal of Greenhouse Gas Control*, vol. 41, pp. 268 – 275, 2015.

[13] A. Berger and A. Bhown, "Optimizing solid sorbents for co_2 capture," *Energy Procedia*, vol. 37, pp. 25–32, 12 2013.

[14] R. Veneman, *Adsorptive systems for post-combustion CO_2 capture*. PhD thesis, 09 2015.

[15] Q. Yu, *Direct Capture of CO_2 from Ambient Air using Solid Sorbents*. PhD thesis, University of Twente, Netherlands, 10 2018.

[16] K. S. Lackner, "The thermodynamics of direct air capture of carbon dioxide," *Energy*, vol. 50, p. 38–46, 02 2013.

[17] H. M. Kvamsdal, G. Haugen, and H. F. Svendsen, "Flue-gas cooling in post-combustion capture plants," *Chemical Engineering Research and Design*, vol. 89, no. 9, pp. 1544 – 1552, 2011. Special Issue on Carbon Capture & Storage.

[18] M. Poudel and B. Dunn, "Greenhouse carbon dioxide supplementation," 2017. Accessed: 2019-02-25.

[19] The Linde Group, "Co_2 for greenhouses." Accessed: 2019-02-25.

[20] B. Messenger, "Co_2 from dutch waste to energy plant to be used in horticultural greenhouses." Waste Management World, Accessed: 2019-02-25.

[21] A. Rijckaert, "Dutch aubergine grower pipes carbon dioxide into greenhouses," 2009. Accessed: 2019-02-25.

[22] D. D. Do, *Adsorption Analysis: Equilibria and Kinetics*. Published by Imperial College Press and distributed by World Scientific Publishing Co., 1998.

[23] F. G. Helfferich, "Principles of adsorption & adsorption processes, by d. m. ruthven, john wiley & sons, 1984, xxiv + 433 pp," *AIChE Journal*, vol. 31, no. 3, pp. 523–524, 1985.

[24] J. E. Wilcox, "Carbon capture using amine-modified carbon nanotubes," 2012.

[25] "Reactor types and catalysts test." Accessed: 2019-04-08.

[26] D. Kunii and O. Levenspiel, "Chapter 3 - fluidization and mapping of regimes," in *Fluidization Engineering (Second Edition)* (D. Kunii and O. Levenspiel, eds.), pp. 61 – 94, Boston: Butterworth-Heinemann, second edition ed., 1991.

[27] A. A. Kareeri, H. D. Zughbi, and H. H. Al-Ali, "Simulation of flow distribution in radial flow reactors," *Industrial & Engineering Chemistry Research*, vol. 45, no. 8, pp. 2862–2874, 2006.

[28] J. C. H. Li, *Radial-Flow Packed-Bed Reactors*. American Cancer Society, 2007.

[29] R. T. Driessen, M. J. Bos, and D. W. F. Brilman, "A multistage fluidized bed for the deep removal of sour gases: Proof of concept and tray efficiencies," *Industrial & Engineering Chemistry Research*, vol. 57, no. 11, pp. 3866–3875, 2018.

[30] N. Frigka, "Experimental study of co_2 and h_2o adsorption," Master's thesis, University of Twente, 2014.

[31] M. J. Bos, V. Kroeze, S. Sutanto, and D. W. F. Brilman, "Evaluating regeneration options of solid amine sorbent for co_2 removal," *Industrial & Engineering Chemistry Research*, vol. 57, no. 32, pp. 11141–11153, 2018.

[32] J. J. Q. van der Linden, "Modelling a supported amine sorbent based multi-stage fluidized bed reactor," Master's thesis, University of Twente, 2018.

[33] M. Bos, T. Kreuger, S. Kersten, and D. Brilman, "Study on transport phenomena and intrinsic kinetics for co_2 adsorption in solid amine sorbent," *Chemical Engineering Journal*, 2018.

[34] R. Bird, W. Stewart, and E. Lightfoot, *Transport Phenomena*. Wiley International edition, Wiley, 2006.

[35] "The engineering toolbox - thermal conductivity." `https://www.engineeringtoolbox.com/air-properties-viscosity-conductivity-heat-capacity-d_1509.html`. Accessed: 2019-08-20.

[36] D. Kunii and O. Levenspiel, "Chapter 11 - particle-to-gas mass and heat transfer," in *Fluidization Engineering (Second Edition)* (D. Kunii and O. Levenspiel, eds.), pp. 61 – 94, Boston: Butterworth-Heinemann, second edition ed., 1991.

[37] F. Incropera, *Fundamentals of heat and mass transfer*. No. v. 1 in Fundamentals of Heat and Mass Transfer, John Wiley, 2007.

[38] M. Bos, S. Pietersen, and D. Brilman, "Production of high purity co_2 from air using solid amine sorbents," *Chemical Engineering Science: X*, vol. 2, p. 100020, 2019.

[39] Q. Yu and D. Brilman, "Design strategy for co_2 adsorption from ambient air using a supported amine based sorbent in a fixed bed reactor," *Energy Procedia*, vol. 114, pp. 6102 – 6114, 2017. 13th International Conference on Greenhouse Gas Control Technologies, GHGT-13, 14-18 November 2016, Lausanne, Switzerland.

[40] "eurostat - statistics explained, statistieken over elektriciteitsprijzen." `https://ec.europa.eu/eurostat/statistics-explained/index.php?title=Electricity_price_statistics/nl`. Accessed: 2019-09-30.

[41] "infogram - hoeveel kost 1 kwh elektriciteit/aardgas?." `https://infogram.com/hoeveel-kost-1-kwh/-elektriciteitaardgas-prijzen-voor-kleine-professionele-afnemers-all-in-exl-btw-1hnq41nlj1/1p63z`. Accessed: 2019-09-09.

[42] T. Buzink, "Investigation of sour gas removal using supported amine sorbent in a pressurized multistage fluidized bed," Master's thesis, University of Twente, 2018.

[43] "Engineers edge, viscosity of air, dynamic and kinematic." `https://www.engineersedge.com/physics/viscosity_of_air_dynamic_and_kinematic_14483.htm`. Accessed: 2019-08-20.

[44] N. I. of Standards and T. (U.S.), *NIST Chemistry Webbook: NIST Standard Reference Database Number 69*. NIST, 2000.

[45] LANXESS energizing chemistry, *PRODUCT INFORMATION LEWATIT® VP OC 1065*, 5 2017.

A Appendix

A.1 List of symbols

Table A.1: List of symbols.

Symbol	Unit	Description
T	°C	temperature
p	bar / Pa	pressure
V	m^3	volume
A	m^2	area
q^*	mol/kg	equilibrium loading
q	mol/kg	sorbent loading
n_s	-	number of available adsorption sites
b	1/bar	adsorption equilibrium constant
$\Delta_r H$	kJ/mol	heat of reaction
R	J/mol.K	gas constant
t	-	Toth isotherm parameter
α	-	Toth isotherm parameter
χ	-	Toth isotherm parameter
Δq_w	mol/kg	working capacity of the sorbent
Δp	Pa	pressure drop
L_m	m	bed thickness
g_c	-	Conversion factor Ergun equation
ϵ_m	-	bed voidage
μ	kg/(m.s)	viscosity
ρ	kg/m^3	density
d_p	nm	particle diameter
u_0	m/s	superficial velocity
ϕ_s	-	particle sphericity
g	m/s^2	gravity force
$t_s toich$	min	stoichiometric time
m_s	kg	mass of sorbent
φ	m^3/h	volumetric flow rate
C	g/m^3	concentration
Q	kJ	heat/energy demand
Cp	kJ/(kg.K)	heat capacity
MW	kg/mol	molecular weight
η	-	efficiency
k	-	C_p/C_v
t	min	time
ϕ	mol/h	molar flow rate
f_b	-	bubble phase

Symbol	Unit	Description
u_t	m/s	terminal velocity
u_s	m/s	solid's velocity
θ	rad	angle
c_d	-	drag coefficient
$\bar{\rho}$	kg/m^3	mean density
G$_s$	kg/(m^2.s)	gas mass flow
Δp_f	Pa	frictional resistence with the pipe wall
d_t	m	pipe/tube diameter
f		friction factor
h	W/(m^2.K)	heat transfer coefficient
L_c	m	characteristic length
λ	W/(m.K)	thermal conductivity
E	J	energy
η_g	-	gas efficiency
C$_{cont}$	€/kg$_{CO_2}$	gas&solid contacting costs
C$_{elect}$	€/kWh	electricity costs
C$_{reg}$	€/kg$_{CO_2}$	regeneration costs
C$_{therm}$	€/GJ	thermal costs
η_s	-	solid efficiency

A.2 List of parameter values

Table A.2: List of parameter values

Symbol	Value	Unit	Reference	First used in
g$_c$	1	-	[42]	equation 2.8
μ(air, 20ºC)	1.83E-05	kg/m.s	[43]	equation 2.8
μ(air, 70ºC)	2.05E-05	kg/m.s	[43]	equation 2.8
ρ(air,20ºC)	1.204	kg/m3	[35]	equation 2.8
ρ(air,70ºC)	0.9996	kg/m3	[35]	equation 2.8
ρ_s	860	kg/m3	Internal SPT Report	equation 2.9
D$_p$	668	nm	[29]	equation 2.8
ϕ_s	1	-	[42]	equation 2.8
Δ_rH	65	kJ/mol	[31]	equation 2.14
MW$_{CO_2}$	0.044	kg/mol	[44]	equation 2.13
Cp$_{sorb}$	1.58	kJ/kg.K	[33]	equation 2.12
Cp$_{CO_2}$	0.85	kJ/kg.K	[33]	equation 2.15
k	1.3	-	[31]	equation 2.16
R	8.314	J/mol.K		equation 2.16
u$_{mf}$	0.09	m/s	[2]	chapter 3
ϵ_{mf}	0.51	-	[2]	equation 2.9
λ_{air}	29.52	mW/m.K	[35]	equation 6.8
λ_s	0.43	W/m.K	[33]	equation 6.10

A.3 Physical properties of Lewatit VP OC 1065

Table A.3: Physical properties of Lewatit® VP OC 1065

Parameter	Unit	Value	Reference
Particle diameter	μm	315-1250	[45]
		668	[29]
Pore diameter	nm	25	[45]
Tortuosity	-	2.3	[45]
Porosity	$m_p^3 ore/m_b^3 ulk$	0.1809	[45]
Density	kg/m^{3}s	769-866	[45]
		860	Internal SPT Report
Surface area	m^2/ g	50	[45]
Heat capacity	kJ/kg/K	1.58	[33]
Thermal conductivity	W/m/K	0.43	[33]

A.4 Energy demands of air compression in the different geometries and reactor types

Working conditions: $T = 21$°C, $p = 1$ atm, $C_{CO_2} = 600$ ppm, $q_w = 0.79$ mol/kg, $\rho_{bed} = 550$ kg/m^3

For 1 kg/h of CO_2: $m_s = 29$ kg and $\varphi = 2.7 \times 10^3 m^3$/h

Pressure drop, ΔP, along the fixed beds determined with the Ergun equation 2.8 and, in the fluidized bed, with equattion 2.9. $Q_{aircomp}$ determined via equation 2.16.

Table A.4: Sensitivity analysis for an axial flow fixed bed, varying the bed thickness, with a fixed amount of sorbent of 29 kg.

			adsorption			desorption		
bed thickness (m)	section (m^2)	diameter (m)	u_0 (m/s)	Δp (Pa)	$Q_{aircomp}$ (kJ/kg)	u_0 (m/s)	Δp (Pa)	$Q_{aircomp}$ (kJ/kg)
5.00E-03	1.05E+01	3.65E+00	7.27E-02	1.88E+01	6.87E+01	1.45E-03	3.54E-01	2.61E-02
2.00E-02	2.62E+00	1.82E+00	2.91E-01	3.53E+02	1.29E+03	5.80E-03	5.69E+00	4.20E-01
3.00E-02	1.74E+00	1.49E+00	4.36E-01	8.73E+02	3.18E+03	8.70E-03	1.28E+01	9.47E-01
4.00E-02	1.31E+00	1.29E+00	5.81E-01	1.69E+03	6.14E+03	1.16E-02	2.29E+01	1.69E+00
6.00E-02	8.72E-01	1.05E+00	8.72E-01	4.43E+03	1.59E+04	1.74E-02	5.17E+01	3.81E+00
8.00E-02	6.54E-01	9.12E-01	1.16E+00	8.98E+03	3.18E+04	2.32E-02	9.23E+01	6.81E+00
1.00E-01	5.23E-01	8.16E-01	1.45E+00	1.58E+04	5.45E+04	2.90E-02	1.45E+02	1.07E+01

Table A.5: Sensitivity analysis for a radial flow fixed bed, varying the bed thickness, with a fixed amount of sorbent of 29 kg and an inner diameter of the cylindrical bed of 30 cm.

			adsorption			desorption		
bed thickness (m)	surface area (m^2)	cylinder height (m)	u_0 (m/s)	Δp (Pa)	$Q_{aircomp}$ (kJ/kg)	u_0 (m/s)	Δp (Pa)	$Q_{aircomp}$ (kJ/kg)
5.00E-03	1.05E+01	1.11E+01	7.27E-02	1.88E+01	6.87E+01	1.45E-03	3.54E-01	2.61E-02
2.00E-02	2.62E+00	2.77E+00	2.91E-01	3.53E+02	1.29E+03	5.80E-03	5.69E+00	4.20E-01
3.00E-02	1.74E+00	1.85E+00	4.36E-01	8.73E+02	3.18E+03	8.70E-03	1.28E+01	9.47E-01
4.00E-02	1.31E+00	1.39E+00	5.81E-01	1.69E+03	6.14E+03	1.16E-02	2.29E+01	1.69E+00
6.00E-02	8.72E-01	9.25E-01	8.72E-01	4.43E+03	1.59E+04	1.74E-02	5.17E+01	3.81E+00
8.00E-02	6.54E-01	6.94E-01	1.16E+00	8.98E+03	3.18E+04	2.32E-02	9.23E+01	6.81E+00
1.00E-01	5.23E-01	5.55E-01	1.45E+00	1.58E+04	5.45E+04	2.90E-02	1.45E+02	1.07E+01

Table A.6: Sensitivity analysis for a fluidized bed during adsorption and fixed bed during desorption, varying the bed thickness, with a fixed amount of sorbent of 29 kg.

			adsorption				desorption (fixed bed)		
bed thickness (m)	section (m^2)	diameter (m)	L_{mf} (m)	u_0 (m/s)	Δp (Pa)	$Q_{aircomp}$ (kJ/kg)	u_0 (m/s)	Δp (Pa)	$Q_{aircomp}$ (kJ/kg)
5.00E-03	1.05E+01	3.65E+00	6.53E-03	7.27E-02	2.69E+01	9.84E+01	1.45E-03	3.54E-01	2.61E-02
2.00E-02	2.62E+00	1.82E+00	2.61E-02	2.91E-01	1.08E+02	3.94E+02	5.80E-03	5.68E+00	4.19E-01
3.00E-02	1.74E+00	1.49E+00	3.92E-02	4.36E-01	1.62E+02	5.90E+02	8.70E-03	1.28E+01	9.46E-01
4.00E-02	1.31E+00	1.29E+00	5.22E-02	5.81E-01	2.16E+02	7.87E+02	1.16E-02	2.28E+01	1.68E+00
6.00E-02	8.72E-01	1.05E+00	7.83E-02	8.72E-01	3.23E+02	1.18E+03	1.74E-02	5.15E+01	3.81E+00
8.00E-02	6.54E-01	9.12E-01	1.04E-01	1.16E+00	4.31E+02	1.57E+03	2.32E-02	9.20E+01	6.79E+00
1.00E-01	5.23E-01	8.16E-01	1.31E-01	1.45E+00	5.39E+02	1.96E+03	2.90E-02	1.44E+02	1.07E+01

A.5 Example of obtaining sorbent loading from breakthrough curve

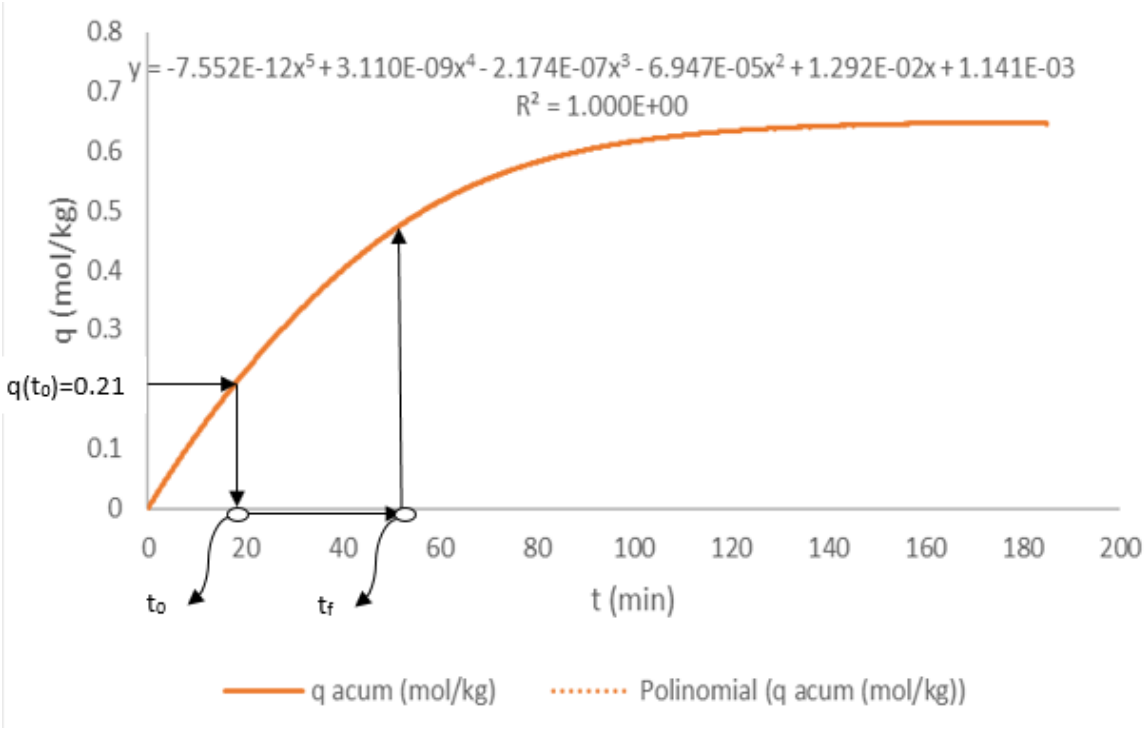

Figure A.1: Example of how the sorbent loading was obtained from breakthrough curve after t_f =residence time in the adsorber, from the breakthrough curve at 600 ppm and 0.23 m/s of air concentration and superficial velocity.

$$CO_{2,obtained}(kg/h) = (q(t_f) - q(t_0)) \times sorbflux \times MW_{CO_2} \tag{A.1}$$

A.6 Calculation of contacting energy in the adsorber

$$E(J/g) = \frac{\Delta P(Pa)}{\eta_g . C_{CO_2}(g/m^3_{air})} \tag{A.2}$$

$$\eta_g = \frac{C_{CO_2}.t - \int_{t_i}^{t_o} C_{CO_2} dt}{C_{CO_2}.t} \tag{A.3}$$

Table A.7: Calculation of contacting energy in the adsorber

stage	u_0 (m/s)	RT (min)	ΔP (Pa)	ti-to (min)	ti-to breakthrough (min)	integral	n_g	E (J/g)
1	0.305	2.4	185.2	0-2.4	10.85-13.25	282.2	0.80	210.4
2				2.4-4.8	13.25-15.65	335.5	0.77	220.5
3				4.8-7.2	15.65-18.05	389.5	0.73	231.8
4				7.2-9.6	18.05-20.45	443.9	0.69	244.5
5	0.22	3.5	276.7	9.6-13.1	30.7-34.2	879.3	0.58	434.7
6				13.1-16.6	34.2-37.7	961.2	0.54	466.0
7				16.6-20.1	37.7-41.2	1041.2	0.50	501.2
8				20.1-23.6	41.2-44.7	1119	0.47	540.9
9	0.12	4.9	284.3	23.6-28.5	96.5-101.4	414.8	0.86	302.3
10				28.5-33.4	101.4-106.3	468	0.84	308.8